THESIS

THE IMPACT OF UPPER TROPOSPHERIC TEMPERATURES AND RADIATION ON IDEALIZED TROPICAL CYCLONES

Submitted by

Benjamin Trabing

Department of Atmospheric Science

In partial fulfillment of the requirements

For the Degree of Master of Science

Colorado State University

Fort Collins, Colorado

Summer 2018

Master's Committee:

Advisor: Michael Bell

Christine Chiu
Siddharth Suryanarayanan

ABSTRACT

THE IMPACT OF UPPER TROPOSPHERIC TEMPERATURES AND RADIATION ON IDEALIZED TROPICAL CYCLONES

Potential intensity (PI) theory predicts that the tropopause temperature acts as a powerful constraint on tropical cyclone (TC) intensity and structure. The physical mechanisms by which the upper tropospheric thermal structure and radiative forcing impact TC intensity and structure have not been fully explored however, due in part to limited observations and the complex interactions between clouds, radiation, and storm dynamics. Idealized Weather Research and Forecasting (WRF) ensembles were conducted using a combination of three different tropopause temperatures (196, 199, and 202 K) with different radiation schemes (full diurnal radiation, longwave only, and no radiation) on weather timescales.

The simulated TC intensity and structure were strongly sensitive to colder tropopause temperatures using only longwave radiation, but were less sensitive using full-radiation and no radiation. The maximum intensity of the longwave only simulations were more sensitive to small boundary layer moisture perturbations in the initial conditions. Colder tropopause temperatures resulted in deeper convection, increased ice mass aloft, and when radiation was included more intense storms on average. Deeper convection led to increased local longwave cooling rates but reduced top of atmosphere outgoing longwave radiation, such that from a Carnot engine perspective, the radiative heat sink is reduced in the stronger storms. It is hypothesized that a balanced response in the secondary circulation described by the Eliassen equation arises from upper troposphere radiative cooling/heating anomalies that leads to stronger tangential winds. The results of this study further suggest that cloud-radiative feedbacks have a non-negligible impact on weather timescales.

ACKNOWLEDGMENTS

First and foremost I must thank Dr. Michael Bell for not only taking me on as a graduate student but for all the support and guidance. I would also like to thank all the members of the Bell research group for their help with debugging, bouncing ideas off of, and most importantly for being great friends. This includes Jon Martinez, Naufal Razin, Ellie Delap, Ting-yu Cha, Chelsea Nam, and Jhordanne Jones. A special thanks also goes to Bruno Melli and Dr. Christopher Slocum for helping me with the seemingly unending stream of fatal errors and programming support. Also I would like to thank Dr. Bonnie Brown for deriving the temperature profiles used in this study.

Additionally I would like to thank the members of my committee Dr. Christine Chiu and Dr. Siddharth Suryanarayanan for their constructive criticism.

Without the support of my friends, family and coworkers this work would not be complete. I would specifically like to thank my wife, Amberly, and son, Oliver, for their support and motivation to keep pushing forward. My gratitude also extends to my parents for their support and inspiring in me the drive to pursue greater knowledge.

This work has been funded by the Office of Naval Research Award N000141613033.

TABLE OF CONTENTS

CHAPTER 1

INTRODUCTION

The 2017 Atlantic Hurricane Season was a destructive and sobering reminder of the power of hurricanes. Hurricanes Harvey, Irma, and Maria all made landfall in the United States as major hurricanes with wind speeds exceeding 50 m s^{-1} (115 mph). Among these record breaking storms a storm that received much less attention was Hurricane Ophelia. Hurricane Ophelia's intensity was underpredicted by nearly every forecast model as it intensified over relatively cold sea surface temperatures (SSTs) (<26°C) and moderate wind shear in the mid-latitudes. Hurricane Ophelia is the farthest East an Atlantic major hurricane has existed on record. One factor that was noted by forecasters to have helped Ophelia to intensify is the anomalously cool temperatures in the upper troposphere (Avila 2017). While there were other factors affecting the intensity of Hurricane Ophelia, the effects of upper tropospheric and lower stratospheric features on hurricane intensity have been largely unexplored and remains an important area of future work (Doyle and Coathors 2017).

Upper tropospheric temperatures have been found to be important for understanding the maximum intensity that a hurricane, or more generically a tropical cyclone (TC), can reach. A potential intensity (PI) theory developed by Holland (1997) was dependent on the use of upper tropospheric temperatures to determine the amount of convective instability; however convective instability was found to be unrelated to the final intensity of an idealized axisymmetric hurricane (Camp and Montgomery 2001; Rotunno and Emanuel 1987; Emanuel 1989). Another theory on the maximum PI that a TC can reach was formulated by Emanuel (1986, 1988). Emanuel (1986) proposed that the maximum intensity was a function of the sensible and latent heat flux from the underlying ocean and the temperature difference between the ocean to the lower stratosphere. The derived equation assumes an axisymmetric and steady-state vortex and bases the formulation on the treatment of a TC as a Carnot heat engine and the balance between frictional dissipation and energy production in the inflowing boundary layer. Bister and Emanuel (1998) updated this theory to include the frictional dissipation of kinetic energy at the molecular scale which increases the kinetic energy density of TCs by roughly 50%. The upper tropospheric temperature is important in this framework for increasing the thermodynamic efficiency of the atmosphere, but understanding the physical mechanism by which this changes the storm dynamics and structure is unclear.

Using PI theory, past studies have shown that upper tropospheric and lower stratospheric temperatures cause changes to TC intensity. Ramsay (2013) analyzed the effects of upper tropospheric and lower stratospheric cooling on TC intensity using a nonhydrostatic axisymmetric cloud resolving model (CM1; Bryan and Fritsch 2002) in radiative convective equilibrium (RCE) over 120 days. They found that maximum intensity of their 2D simulated TCs increased at a rate of 1 m s^{-1} per Kelvin cooling and attributed this to the thermal efficiency change. Wang et al. (2014) used the Advanced Weather Research and Forecasting (WRF; Skamarock and Coauthors 2008) model to simulate how tropopause temperatures affect the intensity of TCs in three dimensions on both short and long timescales in RCE. The maximum intensity of their 3D TCs was found to increase by ~.5 m s^{-1} per Kelvin cooling on both short and long time scales but found no structural difference between the TCs besides an upward shift in the outflow jet. The hypothesized difference between the rate of intensification per degree of tropopause temperature for these two studies was likely due to the model (3D vs. 2D axisymmetric). These studies validate the dependence of PI on upper tropospheric temperatures but do not specifically diagnose the physical mechanisms that causes this dependence.

Two of the many assumptions in PI theory are that a TC at maximum intensity is axisymmetric and in a steady-state. A more in depth description of the assumptions that go into this theory will be discussed in Section 1.2. The steady-state assumption implies that a TC must be in a sort of statistical or radiative equilibrium which may not be practical for real cases like Ophelia as noted by Hakim (2011). However a TC in a slow intensification or when the local time tendency is small to be in a quasi-steady state framework such as in Bell and Montgomery (2008) can be considered to use PI theory to diagnose the role of upper tropospheric temperatures on intensification. The evaluation of upper tropospheric temperatures on PI theory has primarily been evaluated on long time scales >100 days (Emanuel et al. 2013; Ramsay 2013). The axisymmetric assumption has constrained past studies to use 2D models to analyze the parameter space (e.g. Rotunno and Emanuel 1987; Bryan and Fritsch 2002; Ramsay 2013). Only recently has PI theory in three dimensions been examined by Wang et al. (2014) but with only a limited focus on short scales. This study showed that tropopause cooling yielded a stronger hurricane on both short and long time scales with slightly different magnitudes. However this study still employed RCE and as such the evaluation of PI theory in a three-dimensional full-physics model has not yet been attempted. PI theory must be understood in a three-dimensional full physics framework to fully incorporate it into the assessment of real-time forecasts like in the case of Hurricane Ophelia.

According to Emanuel's PI theory, the upper tropospheric temperatures are important for modifying the thermodynamic efficiency of the atmosphere and was considered by forecasters at the National Hurricane Center when making their forecast for the intensity of Hurricane Ophelia (Avila 2017). In this study high-resolution three-dimensional full-physics models are used to attempt to diagnose the physical mechanisms behind why changing upper tropospheric temperatures modify TC intensity. The simulations are focused on weather timescales of a few days in order to both diagnose this physical mechanism and to investigate the use of PI on understanding TCs on short time scales. Radiation is important because of its potential to alter the upper tropospheric temperature structure and should be considered . The effects of radiation will be assessed through the balanced response to diabatic heating in the secondary (transverse) circulation described by the Eliassen model (Eliassen 1952). It is hypothesized that while changes to the thermodynamic efficiency and height of the atmospheric system may be important for understanding changes to PI from upper tropospheric temperatures, it is likely the anomalies in the radiative tendencies that induce anomalous secondary circulations that intensify the vortex.

The thesis is outlined as follows. A thorough discussion of the work of past studies on radiation in TCs, PI and the Carnot model, and the Eliassen model will be offered. Chapter 2 will detail the setup of the idealized simulations. Chapter 3 will show how the upper tropospheric temperatures impacted the intensity of the idealized simulations before analyzing the effects of radiation. Chapter 4 will address the structural differences between the simulations. Chapter 5 will discuss the variability of the longwave only simulations due to subtle moisture perturbation. Chapter 6 will detail how the results of this study fits into the Carnot model and Chapter 7 will summarize the conclusions from this work.

1.1 Radiation in Tropical Cyclones

Past studies have frequently neglected the effects of radiation on hurricanes because of the complexity it adds to the system (e.g. Nolan 2007). This includes short wavelength solar radiation and long wavelength infrared radiation emitted by Earth. Shortwave radiation has a net heating effect on the atmosphere while longwave radiation can have a net heating or net cooling effect on the atmosphere depending on the radiative flux divergence within an atmospheric layer. Both types of radiation contribute to the temperature balance of the atmosphere and can positively or negatively affect TC intensity and structure in various ways on both short and long time scales. This includes the generation and maintenance of cloud layers shown by Rogers and Karacin (1992).

Radiation is believed to be the cause of diurnal cycles in convection; however the mechanisms that drive this cycle in TCs are still being debated (Dunion et al. 2014). Past studies have proposed three primary mechanisms by which radiation affects TC intensity over the diurnal cycle. These mechanisms include differential heating between cloudy and cloud-free regions (Gray and Jacobson 1977; Craig 1996; Nicholls 2015), large-scale destabilization from longwave cooling (Dudhia 1989; Melhauser and Zhang 2014; Sui et al. 1998), and changes in instability from radiative differences between cloud base and cloud top (Godbole 1973; Xu and Randall 1995). Tang and Zhang (2016) suggested that all three mechanisms may play a role in modifying hurricane intensity and structure at different stages of development.

Gray and Jacobson (1977) hypothesized that the diurnal cycle of deep cumulus convection in the tropics was driven by differential heating/cooling of cloudy and cloud-free areas. At night, radiative cooling in clear air promotes subsidence which increases low-level convergence into adjacent cloudy regions. Craig (1996) found similar results using an axisymmetric model with coarse resolution indicating that the extent of the cloud cover would then modulate the TC intensification. Nicholls (2015) showed that radiatively induced circulations influence relative humidity, static stability, and low level circulations with the primary mechanism for early intensification of TCs being the differential cooling between cloudy and cloud-free areas. Emanuel (1989) used the nonhydrostatic axisymmetric model of Rotunno and Emanuel (1987) to show a similar circulation but noted that the function of radiative cooling in the outer core was to permit subsidence of dry air to counteract the moistening effects of low-precipitation-efficiency clouds.

Dudhia (1989) found that the effects of longwave radiation were to cause stronger and deeper convection in a simulated mesoscale convective system (MCS) by continually destabilizing the clear air atmosphere. Melhauser and Zhang (2014) extended this work to the pregenesis area of Hurricane Karl (2010) finding that clear air cooling by longwave radiation allowed for a deeper vortex to form though increasing relative humidity. It was noted in their study that simulations with only longwave radiation intensified the fastest while simulations with only shortwave radiation did not develop. Because the simulations did not develop with only shortwave radiation, longwave radiation must be critical for offsetting the effects of shortwave radiation to create a conducive environment for TC development and intensification. Sui et al. (1998) found that increases in nocturnal rainfall of tropical oceanic convection was a direct response to increases in precipitable water from radiative cooling.

Gray and Jacobson (1977) initially proposed that radiative cooling at the top of the troposphere should not be sufficient to cause a large diurnal cycle in deep convection. The magnitude of cloud top destabilization from longwave cooling is small compared to that of latent heat release, however it was shown to have a non negligible impact by Godbole (1973) depending strongly on the thickness of the clouds. Xu and Randall (1995) found that radiative destabilization is a two step process in which first the radiative destabilization enhances turbulent scale motions nearly instantaneously, and after some time the cloud-scale motion is enhanced. Radiative destabilization was found to be especially important for thin anvil clouds which became more active and lasted longer in their simulations.

Modeling studies have shown that radiation acts to modify not only the intensification rates of TCs but also the structure (Fovell et al. 2010; Bu et al. 2014; Nicholls 2015; Tang and Zhang 2016). Fovell et al. (2010) showed how the complex interactions between radiation and cloud microphysics can influence the heating patterns affecting TC structure and tracks. Bu et al. (2014) varied the cloud radiative forcing in WRF to show that the weak primarily longwave heating in the anvil region of TCs is responsible for stronger upper tropospheric radial outflow and a broader tangential wind field. Nicholls (2015) and Tang and Zhang (2016) also showed that the effect of both shortwave and longwave radiation was to enhance the size of the hurricane vortex. Partially due to some focus on tropical cyclogenesis, past studies have not found any relationship between the type of radiation employed and the peak intensity of their simulated storms (Sundqvist 1970; Craig 1996; Fovell et al. 2010; Melhauser and Zhang 2014; Bu et al. 2014; Nicholls 2015; Tang and Zhang 2016). Fovell et al. (2016) noted that the relationship between cloud microphysics, radiation, and storm intensity were model dependent and an important issue for future work.

1.2 Potential Intensity and the Carnot Model

The PI of a TC is a powerful theoretical upper bound on intensity that has been depends solely on environmental factors. The Statistical Hurricane Intensity Prediction Scheme (SHIPS; DeMaria and Kaplan 1994) is a statistical model using persistence, climatological, and synoptic predictors in a multiple regression scheme to forecast intensity. The difference between a TC's current intensity and the PI was found to be the most important predictor in SHIPS (DeMaria and Kaplan 1999). The importance of PI in forecasting TC intensity is evident by SHIPS and as such more work needs to be conducted to assess its sensitivities and limitations.

The most prominent PI theory that has withstood the test of time is that of Emanuel (1986, 1988). PI is derived primarily from the balance between frictional energy dissipation and energy production in the inflowing boundary layer from fluxes of moist enthalpy. In this framework it is assumed that the atmosphere is neutral to slantwise convection, in hydrostatic balance, that there is gradient wind balance, and as previously mentioned that the TC is axisymmetric and in a steady-state. The resulting PI of a TC can then be conceptualized as a Carnot heat engine which was first hypothesized by Kleinschmidt (1951). The heat engine is driven by the thermodynamic disequilibrium between the tropical oceans and the atmosphere (Emanuel 1986). The equation to a Carnot heat engine assumes the approximation of no radial temperature gradients in the mixed layer and no dissipation of energy except for in the inflow and at large radii in the outflow (Emanuel 1988). The Emanuel PI equation was modified by Bister and Emanuel (1998) by the inclusion of dissipative heating which increased the theoretical maximum wind speeds in TCs by about 20%. After the inclusion of dissipative heating the following equation for PI is attained.

$$V^2 = \frac{T_s - T_0}{T_0} \frac{C_k}{C_D} (k^* - k) \tag{1.1}$$

Where V^2 is the magnitude of the surface wind speed, T_s is the ocean surface temperature, and T_0 is the temperature of the outflow. C_k and C_D are the exchange coefficients of momentum and enthalpy and k^* and k are the saturation enthalpy of the sea surface and the actual enthalpy of the boundary layer air. It follows from Eq. (1.1) that by increasing the upper tropospheric temperatures, the value of $\frac{T_s - T_0}{T_0}$, which is related to the thermodynamic efficiency, would be reduced and thus the magnitude of the surface winds would also be reduced. If the temperature of the outflow is conversely cooled, the opposite would happen and the surface winds would theoretically increase. It is from the thermodynamic efficiency that the upper tropospheric temperatures were shown to modify TC intensity by Ramsay (2013) and Wang et al. (2014).

The Carnot model for a hurricane is characterized through the secondary circulation. A closed Carnot cycle is represented as a rectangle on a temperature-entropy diagram. The Carnot cycle consists of four steps which are isothermal expansion, adiabatic expansion, isothermal compression, and adiabatic expansion shown in Fig. 1.1 in both height-radius and temperature-entropy space. These four steps are equated to a TC by first considering the isothermal expansion of air as radial inflow transports parcels at constant T_s from outer radii towards the low pressure center. Along the path towards the center, parcels gain moist entropy from wind induced sensible and latent heat fluxes from

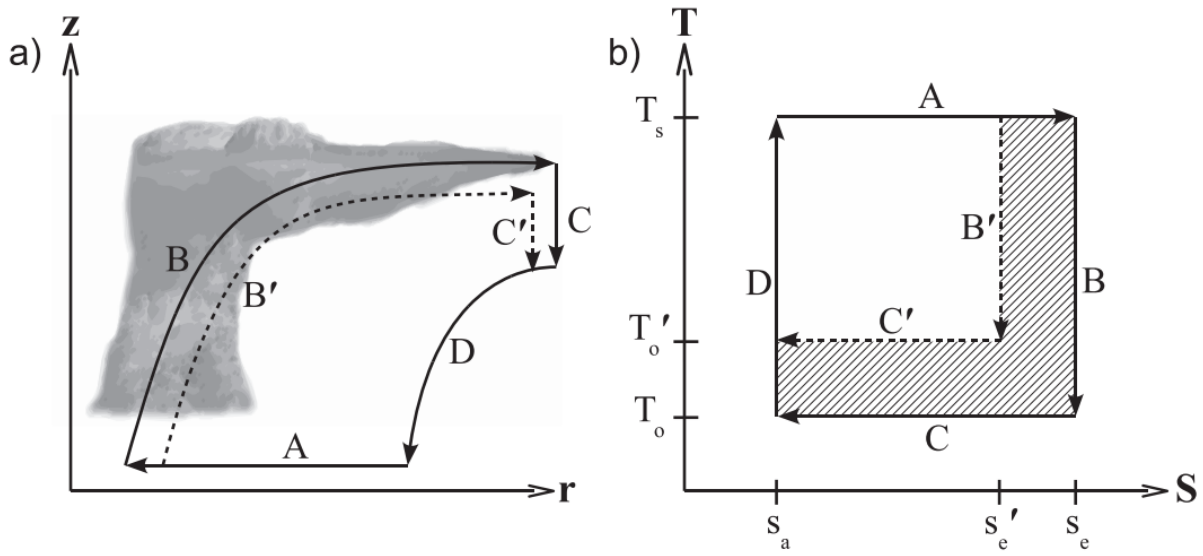

FIG. 1.1. Adapted from Tang and Emanuel (2010). The secondary circulation of an idealized TC (a) and the corresponding entropy temperature diagram (b). Lines A-B-C-D are the four steps of the Carnot cycle representing isothermal expansion, adiabatic expansion, isothermal compression, and adiabatic compression.

the ocean. Parcels then turn vertical in the eyewall and expand adiabatically following a line of constant moist entropy or angular momentum surface. Following a constant moist entropy surface the parcel must flow radially outward to an approximated outflow temperature T_0. Parcels then subside at T_0 isothermally due to a balance between radiative cooling and subsidence warming losing entropy as it descends. The final leg in the closed cycle is then adiabatic compression as the parcel subsides back down to the surface at large radii away from the storm center. In the adiabatic compression leg air is continually cooled by radiation; however, because the environmental temperature profile is moist adiabatic, the amount of radiative cooling is the same as if the air were saturated and descending moist adiabatically (Emanuel 2004). The larger the difference between T_s and T_0 then represents a larger area in the temperature-entropy diagram which represents the amount of work available to power the winds against frictional dissipation (Tang and Emanuel 2010).

The outflow temperature, T_0, has been defined differently over the years (e.g. Emanuel 1986, 2012). It was originally thought to be constant as angular momentum surfaces emanating out of the boundary layer in a troposphere that is neutral to moist convection would reach above the tropopause into the nearly isothermal stratosphere Emanuel (1986). Bister and Emanuel (1998) noted that T_0 should be defined as the temperature along the angular momentum surface that passes through the locus of maximum winds at the point where the tangential velocity is zero. Emanuel and Rotunno (2011) showed

that this definition of outflow temperature is very close to the ambient tropopause temperature which was used by Emanuel et al. (2013) to show that tropopause layer cooling was responsible for an increase in theoretical PI over the past decades. Emanuel and Rotunno (2011) and Emanuel (2012) showed that the assumption of a constant outflow temperature in an idealized convective allowing axisymmetric model is not justified. By relaxing the constant outflow temperature constraint, they showed that the thermal stratification of the outflow layer set by the Richardson number may be a controlling factor for TC intensity change.

In the Carnot model, the energy sources are confined to the addition of moist entropy in the boundary layer inflow and by radiative cooling of the outflow layer (Emanuel 1986). It is not well understood how radiation may interact with the tropopause temperature to change PI. Although Emanuel (1989) notes that radiative cooling is necessary for a TC to maintain a quasi-steady vortex, it is assumed through the Carnot model that longwave radiation and subsidence warming will balance each other during the isothermal compression leg and radiative effects in the adiabatic compression leg is offset by moisture differences (Emanuel 1997, 2003, 2004). It is not clear how balance is maintained with nonlinear feedbacks from radiation and changes to the outgoing longwave radiation (OLR) at different temperature levels. It is also assumed that radiative effects are essentially negligible during the other three legs, including the adiabatic expansion leg where air travels radially outward in the outflow. Newtonian cooling schemes were used in both Ramsay (2013) and Wang et al. (2014) which prevented any cloud-radiative feedbacks within the TCs. In order to completely understand how upper tropospheric temperatures affect PI, the cloud radiative effects must also be understood.

1.3 Eliassen Model

Eliassen's seminal work in 1952 describes the balanced response to a heat or angular momentum source for the secondary circulation of a stable circular vortex. The Eliassen model is not time dependent because it describes the balanced response to a heat source at a given time; however, it can be continuously coupled with the tangential momentum equation to describe an evolving balanced vortex. The Eliassen model has been used to show the importance of diabatic heat sources in driving the secondary circulation of TCs and maintaining the ring structure of TCs (Wu et al. 2016). Willoughby (2009) derived an equation for the toroidal component of vorticity induced by time varying heat sources which is analogous to the Eliassen equation. This equation was used to show that inertia-buoyancy waves radiate into the environment when the period of forcing in the vortex core is less than one pendulum

day. It was also noted that only steady forcing intensified the vortex permanently and that low frequency forcing caused Eliassen-like secondary circulation intensifications during the heating phases and weakening during the cooling phase that had little net effect on intensity.

Navarro and Hakim (2016) used WRF to analyze the the TC diurnal cycle and found by Fourier analysis that TC intensity is roughly 1 m s^{-1} stronger in the mid-morning compared to the evening. This work hypothesized that the TC diurnal cycle is a response from the solar heating in the outflow and an increase in latent heating indirectly from longwave cooling in the boundary layer. The derivation by Willoughby (2009) was subsequently used in Navarro et al. (2017) to analyze the balanced response of an axisymmetric TC to diurnal heating using the previously found heating profiles. The response of the diagnostic and Eliassen equation and their CM1 simulations showed that the location of heating caused a local overturning response in the secondary circulation. Periodic upper-level heating modified the upper-level outflow but did not modify the overall strength of the simulated hurricane. The low level forcing that was indirectly related to the longwave cooling however was able to intensify the hurricane. Navarro et al. (2017) did not include variations in static stability in the upper troposphere and was not able to resolve other cloud-radiative feedbacks.

CHAPTER 2

METHODS

Due to the complicated interactions between clouds, radiation, and storm dynamics, idealized numerical simulations are conducted. The Advanced Research WRF model (ARW; version 3.7.1) is employed which is a three-dimensional full-physics model (Skamarock and Coauthors 2008). First, thermodynamic profiles are derived based on observations as the initial condition for the simulations. The derived thermodynamic profiles will give the idealized simulations a realistic environment to develop in. Using similar profiles with different upper tropospheric temperatures will allow the relationship between TC intensity and structure to the temperature profile differences to be assessed. Then the model physics will be modified to address the sensitivities to radiation and random moisture perturbations.

In order to make the idealized simulations realistic, three environmental input soundings are derived from the National Centers for Environmental Prediction (NCEP) Climate Forecast System Reanalysis (CFSR; Saha and Coathors 2010). Since the goal of this study is understanding the response of TCs to upper tropospheric temperatures, the tropopause temperature and height dependence on latitude is utilized. The tropopause descends and warms when moving poleward from the equator (Seidel et al. 2001). Monthly temperature products were averaged between 144E and 180E from June, July, and August. Average are then taken across latitudinal bands of 10N, 20N, and 30N. This results in mean soundings for 10N, 20N, and 30N with tropopause temperatures of 196.3 K, 199.9 K, and 202.9 K respectively. These three thermodynamic profiles were then averaged below 200 hPa in order to isolate only the upper tropospheric and stratospheric differences. Fig. 2.1 shows the initial sounding for each case with the cold point tropopause (CPT) pressure level highlighted by the dashed black line. Each profile is conditionally unstable and employs the same dew point temperature profile that has no moisture above 200 hPa. The tropical tropopause layer (TTL) has been shown to be well characterized with an upper boundary as the CPT temperature (Gettelman and Forster 2002).

Idealized WRF simulations with two-way nested doubly-periodic domains were utilized with 18, 6, and 2 km resolution in the horizontal. The outer domain extended 5,400 km in the horizontal and the model top reached 25 km with 30 vertical levels. Experiments were conducted with no land and SSTs fixed at 301 K. Models were initiated with zero background flow and employed an F-plane approximation (F=0.5*10^{-5} s^{-1}). Simulations were focused on weather time scales lasting eight days and initialized with a weak vortex based off Rotunno and Emanuel (1987).

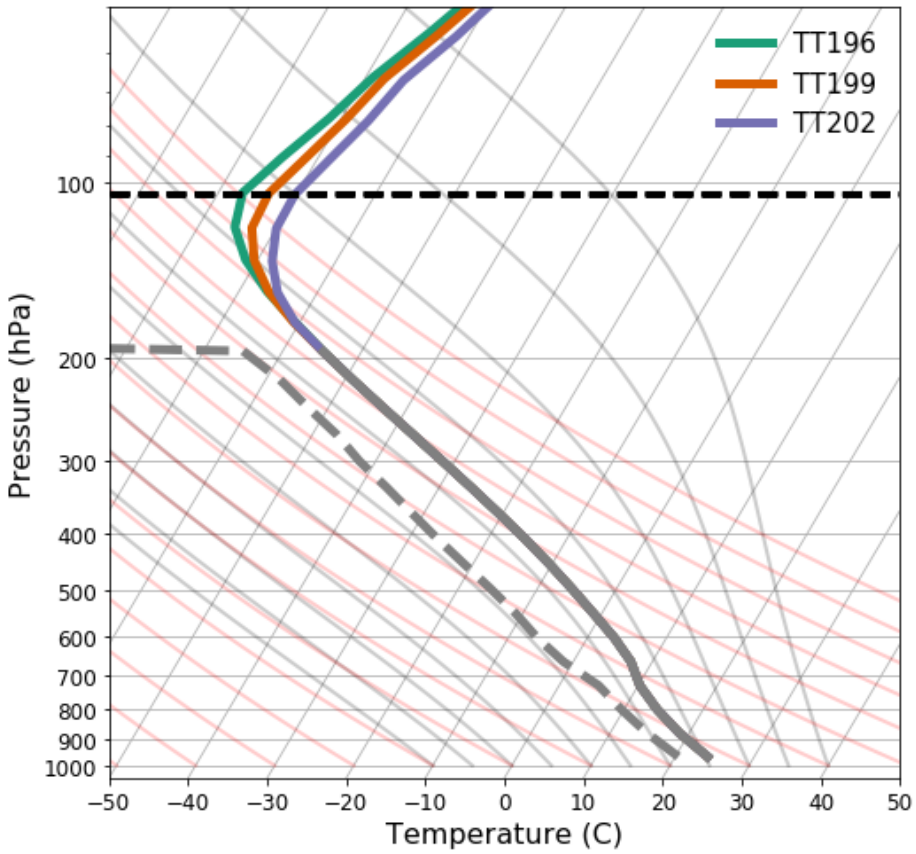

FIG. 2.1. Thermodynamic profile derived from NCEP CFSR data for each experiment on a Skew-T/Log-P diagram. Below 200 hPa the profiles are averaged together indicated by the thick gray line. The gray dashed line indicates the dewpoint temperature profile. Horizontal black dashed line indicates the CPT pressure level.

Simulations were performed using the Thompson aerosol-aware microphysics scheme (Thompson and Eidhammer 2014) and the Yonsei University planetary boundary layer scheme (Hong et al. 2006). The coarse outer domain included the New Tiedtke convective parameterization (Tiedtke 1989). The Rapid Radiative Transfer Model (RRTM) was used for longwave radiation. RRTM is a simplistic but accurate scheme that accounts for multiple bands and microphysics species (Mlawer et al. 1997). The Dudhia shortwave radiation (Dudhia 1989) is also a simplistic but accurate radiation scheme employed in the simulations.

Approximately 3.3 K differentiates the CPT between each input sounding. This variation is small compared to the range of CPT values Wang et al. (2014) implemented. In the RCE environment of their experiment, tropopause temperatures of 195 K and 200 K showed no differences in peak tangential winds over the initial eight days with differences occurring in the time means over 100 days. On short

time scales it is expected that the idealized TC's intensity will be sensitive to stochastic changes in convection. Therefore due to model sensitivities and the range of the derived thermodynamic profiles, an ensemble approach was taken. An ensemble will also result in better understanding of model variability in increase confidence in the results.

For each input sounding, 15 ensemble members were simulated using the method employed by Van Sang et al. (2008). A random water vapor mixing-ratio perturbation between ± 0.5 g kg^{-1} was introduced to the lowest pressure level in order to address model sensitivities. Introducing stochastic perturbations provides a spread of hurricane intensities after t=48-72h of model integration. The delay in variability of ensemble members indicates a limited moisture perturbation effect on the spin-up of the vortex and the environment. The simulations will herein be referred to by their CPT temperatures at model initialization (i.e. TT196, TT199, TT202) and the ensemble mean will be shown unless otherwise noted.

Three sets of experiments were conducted using the three derived thermodynamic profiles. One experiment includes both shortwave and longwave radiation and will be referred to as "Fullrad". The second experiment includes turning off the shortwave heating from the sun and will be therefore referred to as "Nightonly". These results were then compared to control simulations without radiation which will be referred to as "Norad". This results in a total of 9 experiments and allows for the analysis of radiative effects not present in past studies that employed Newtonian cooling schemes in RCE.

By comparing each hurricanes' intensity as a function of the thermodynamic profile and radiation, a better understanding of how upper tropospheric temperatures affect peak intensity will be gained. It is important to remind the reader that each simulation was conducted on an F-plane with the same Coriolis force. Although differences in latitude were used to attain the thermodynamic profiles, these simulations do not necessarily depict latitudinal dependencies in hurricane intensity.

CHAPTER 3

INTENSITY

I will now analyze the effects of upper tropospheric temperatures on the maximum 10-m winds of the simulated TCs. Fig. 3.1 shows the evolution of the maximum 10-m wind speeds for all the experiments. The bold lines are the ensemble means and the hatched areas are the ensemble spread of ± one standard deviation. The hatched areas therefore indicate the variability in maximum 10-m winds due to the random water vapor mixing ratio perturbations. The general characteristics of Fig. 3.1 will be discussed here and the the details of the individual experiments will be discussed in the following two sections.

Fig. 3.1 shows that each of the simulations undergoes a short spin-up time period before rapidly intensifying into an intense TC exceeding 70 m s^{-1}. The Nightonly simulation intensifies the fastest followed by the Fullrad and the Norad simulations. The effect of radiation on intensification rate has been shown by previous studies and can be attributed to differences in relative humidity and large-scale destabilization (Melhauser and Zhang 2014; Nicholls 2015). The Nightonly simulations also attain the strongest maximum 10-m wind speeds while the Fullrad and Norad simulations reach similar peak

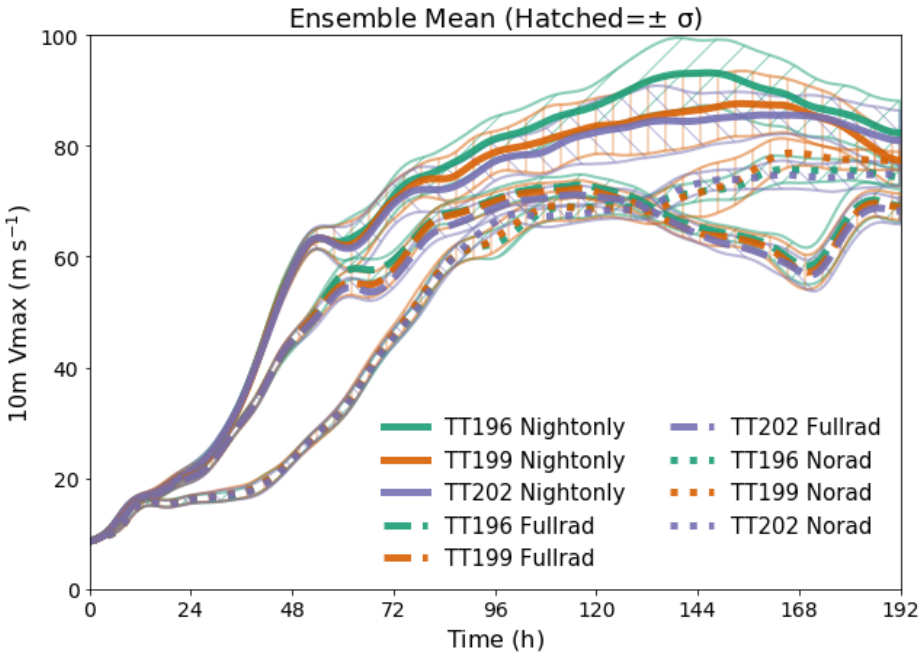

FIG. 3.1. Maximum 10-m wind speeds ensemble mean for Nightonly (solid), Fullrad (dashed), and Norad (dotted) simulations with hatched ± standard deviation. Smoothed using 10 iterations of a 1-2-1 filter with weights of .25, .5, and .25 respectively.

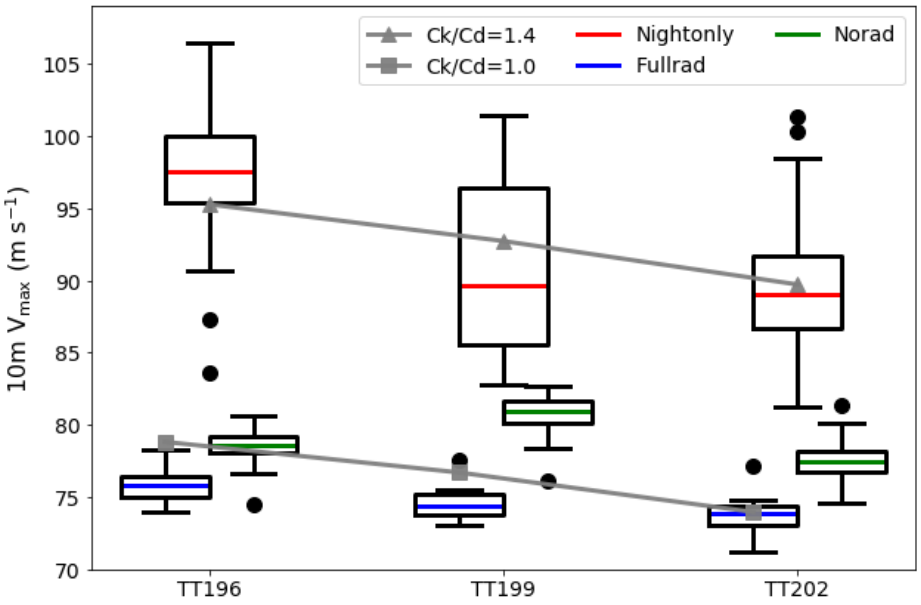

FIG. 3.2. Boxplot of Vmax for each ensemble member for the Nightonly (red), Fullrad (blue), and Norad (green) simulations. The colored lines are the median. The 25th and 75th interval is indicated by the box with outliers in filled black circles where the distance between the box was greater than 1.5 times the width of the box. Gray lines are the theorized intensity based on PI (Bister and Emanuel 2002) using different relationships between the ratio of exchange coefficients.

intensities. Over the first two days for the Nightonly and Fullrad and three days for the Norad simulations, there exists no discernible difference between V_{max} of the TT196, TT199, and TT202 ensemble means. The lack of differences over the early time periods indicates that upper tropospheric temperatures had little effect on the spin-up of the TC vortex. There also exists nearly no difference in the standard deviations indicating that the random moisture perturbations to the boundary layer also had negligible effects on TC genesis and early intensification. The variability of the experiments increase at later times with the Nightonly simulations showing the largest spread and the Fullrad simulations showing the smallest variability.

We can directly compare the theoretical PI and the maximum intensity of the idealized simulations by analyzing the boxplot in Fig. 3.2. The boxplot shows the maximum 10-m winds in the inner domain of the simulations with the median of each experiment highlighted by the colored lines. The expected theoretical PI calculated using a modified form of Eq. 1.1 from Bister and Emanuel (2002) for the given environment is shown in the gray lines. The gray line with the squares is the expected PI when it is assumed that the ratio of exchange coefficients (C_k/C_D) is unity and the line with triangles is when $C_k/C_D = 1.4$. In the Nightonly simulations and the Fullrad simulations there is an increase

in maximum 10-m winds with decreasing upper tropospheric temperatures. In the Norad simulations TT199 is the strongest and not TT196 which is predicted by Eq. 1.1. The theoretical PI lines show a different slope for the increase in maximum 10-m winds per Kelvin of upper tropospheric cooling in the Fullrad simulations but cannot be determined in the Nightonly simulations due to the large ensemble variability. Figs. 3.1 and 3.2 are introduced here but will be analyzed in more depth in the next two sections.

3.1 Upper Tropospheric Temperature Impacts

The control simulations in which there is no radiation will now be analyzed. Similar to other past idealized studies radiation can be turned off to examine the upper tropospheric temperatures in the simplest framework (e.g. Nolan 2007). Radiation, particularly longwave radiation, plays an important role in maintaining the temperature balance of the atmosphere Emanuel (1989). As such by neglecting radiation, the environment will continue to be warmer than it would otherwise be with the inclusion of radiation and therefore affect convective instability. On short time scales, however, it is assumed that the differences between the ensembles will be directly attributed to the upper tropospheric temperature differences.

Again Fig. 3.1 shows the maximum 10-m wind speeds for all the experiments with the simulations without radiation pictured with dotted lines. After three days the ensemble means begin to diverge slightly and then vacillate around each other. The standard deviations increase as the small moisture perturbations have a larger effect on the TC intensity at these later times, likely due to convective feedbacks. No clear relationship exists between the TC intensities and upper tropospheric temperatures as TT199 becomes the most intense after t=144h. Because TT199 was the strongest, the simulations with the coldest upper tropospheric temperatures (TT196) did not have the strongest TCs which is anticipated by PI theory. Due to the variability of the intensities and the small difference between the ensemble means, the Null hypothesis that the ensemble means are the same cannot be rejected at the 95% confidence interval using a two-sided T-test. Since it cannot be stated statistically that the intensities are different, upper tropospheric temperatures had very little effect on the intensity of the Norad ensembles.

The theoretical PI and the maximum intensities of the experiments are shown in Fig. 3.2 with the Norad simulation medians indicated by the green lines. It is clear from this figure that the simulations do not provide the expected increase in PI caused by colder upper tropospheric temperatures. It is unlikely that WRF depicts a critical point at TT199 where a local maximum in intensity is found for that

particular thermodynamic profile. The relationship between upper tropospheric temperatures and PI is therefore not consistent with PI theory without the effects of radiation.

3.2 Radiative Impacts

Both longwave and shortwave radiation will modify the environmental thermodynamic profile from the start of the simulation. For this reason the maximum 10-m wind speeds shown in Fig. 3.1 for the Fullrad and Nightonly experiments exhibit different intensification rates compared to the Norad experiment. This means that when comparing these experiments to the control, the radiative impacts on the large-scale environment must also take into consideration. The Norad experiment showed that upper tropospheric temperatures have no clear relationship to PI theory. The combined effects of radiation with the upper tropospheric temperatures on short time scales will now be addressed.

After 48 hours the intensity of the Fullrad and Nightonly experiments become more distinct with the Nightonly simulations reaching stronger maximum intensities. The intensification rate of the Nightonly simulations slow down after the intensity reaches 70 m s^{-1} with ensemble members then intensifying at different rates. The TT196 simulations continue to intensify at faster rates than TT199 which in turn intensifies slightly faster than TT202 simulations. This results in a time lag of roughly 12 hours between when each of these ensemble means reaches its peak intensity. A time lag in maximum tangential wind speeds was also shown by Wang et al. (2014) during the first eight days of their simulations in RCE but not discussed. The magnitude of this time lag is different from this study which is likely due to both differences in model initial conditions and the use of longwave radiation. The time lag in maximum wind speeds caused by the different intensification rates may be due to longwave radiative tendencies since this time lag is not evident in the Fullrad or Norad experiments.

The strength of the maximum 10-m winds in the Fullrad experiment are weaker than the Nightonly experiments but stronger than the Norad experiment over the first five days. The ensemble means of TT196, TT199, and TT202 do not show substantial differences between each other like in the Nightonly experiment. Instead, TT196 remains slightly stronger than TT199 which in turn is slightly stronger than TT202 at all times after t=48h. After peaking in intensity around t=108h, the Fullard storms begin to weaken due to the formation of a secondary wind maximum. The formation of a secondary wind maximum is associated with an eyewall replacement cycle (ERC) which weakens the overall intensity of the storm but expands the tangential wind field. The secondary eyewall formation curiously occurred in each of the ensemble members and it is unclear whether the Fullrad storms would have eclipsed

the peak intensity of the Norad simulations had the ERC not occurred. The effect of radiation on the possible formation of secondary eyewalls is outside the scope of this study but is an interesting topic for future work.

The Nightonly ensembles exhibit more variability after 48 hours compared to the Fullrad and Norad ensembles. The increase in variability in the Nightonly experiments means that longwave radiation interacted with convection in different ways due to the small moisture perturbations. The sensitivity of the Nightonly simulations to small moisture perturbations will be discussed in more detail in Chapter 5. The shortwave heating in the Fullrad simulations appears to have helped to counteract this effect since the Fullrad ensembles exhibit very little variability due to the moisture perturbations. A two-sided T-test reveals statistically significant differences only at certain times in the Fullrad simulations because even though the variance is small, the differences between the TT196 and TT202 means are small. In the Nightonly simulations, there are much larger differences in the means but also larger variances in the ensembles means between the TT196 and TT202. TT196 and TT202 are statistically different at the 95^{th} confidence level using the same two-sided T-test; however, the Null cannot be rejected when comparing TT199 and TT202. Therefore the response of the simulated TC intensity to the same difference in upper tropospheric temperatures in the Nightonly case may not be linear.

To better characterize the variability of V_{max} and how the idealized simulations compared to PI theory, the box-and-whiskers plot of V_{max} for every experiment shown in Fig. 3.2 are again analyzed. Nightonly simulations were more sensitive to the boundary layer moisture perturbations while the Fullrad and Norad simulations were less so. Each Nightonly experiment had ranges exceeding 15 m s^{-1} while the Fullrad and Norad experiments had ranges closer to 5 m s^{-1}. This makes comparing PI rather difficult, particularly for the Nightonly experiments. By adjusting the ratio of the non-dimensional surface exchange coefficient for enthalpy and the drag coefficient (C_k/C_D) to 1.4, similar ensemble V_{max} and PI values are attained. It must be noted this ratio is much higher than expected based on observations from six missions into hurricanes Fabian and Isabel during the 2003 Coupled Boundary Layers Air-Sea Transfer (CBLAST) field campaign. From these observations Bell et al. (2012) found an average C_k/C_D of 0.4 with a range of 0.17 to 1.05 by adding and subtracting one standard deviation. In the Fullrad experiments, the relationship between V_{max} and upper tropospheric temperatures appears linear but the slope is slightly different from PI. In the Nightonly experiments, the relationship also appears

linear; however, an exponential relationship cannot be resolved by these three points. Since the No-rad simulations do not show an increase in maximum wind speeds with colder upper tropospheric temperatures, radiation is therefore important to our understanding PI theory.

As previously shown, the relationship between V_{max} and upper tropospheric temperatures is sensitive to the radiation scheme. If the ensemble means are considered for the experiments with radiation, approximate relationships of -0.3 m s^{-1} K^{-1} for Fullrad and ~-1.3 m s^{-1} K^{-1} for Nightonly experiments result. PI calculated using Bister and Emanuel (2002) has a PI to outflow cooling relationship between ~0.5-0.9 m s^{-1} K^{-1} for $C_k/C_D = 0.5$ - 1.5 at a constant SST=301 K. The range from the simulations is larger than expected from PI theory and the ~0.4-0.5 m s^{-1} K^{-1} of cooling for PI increase found by Wang et al. (2014). These differences in rates are likely due to the treatment of radiation and cloud-radiative feedbacks in addition to the differences in time scales.

The ensemble means of this study agree with PI theory when radiation is included such that the cooling of upper tropospheric temperatures causes an increase in maximum V_{max} and a warming results in reduced maximum V_{max}. However, when radiation is removed from the model, this relationship is not present over the eight day simulations. The magnitude of the relationship is sensitive to the radiation scheme in addition to the small boundary layer moisture perturbations present in each simulation. The radiation scheme and the upper tropospheric temperatures are thus important to consider for their role in modulating TC intensity on timescales of eight days. The sensitivity of the upper tropospheric temperatures to radiation should be accounted for when applying PI theory to real cases on weather time scales.

CHAPTER 4

STRUCTURE

4.1 UPPER TROPOSPHERIC TEMPERATURE IMPACTS

To diagnose how upper tropospheric temperatures affect the structure of idealized TCs the characteristics of the simulations without radiation must be understood. The resulting differences between the storms can thus be directly attributed to the temperature differences. First the early time periods (t=24-96h) will be presented where individual ensemble members for each experiment are consistent and all simulations are intensifying. The lack of intensity differences during these times will allow a better comparison of storm structures that caused differences in the intensification rates at later times. The structure near peak intensity, between t=96-168h, will then be analyzed to understand how differences in structure evolved to create TCs of various intensities.

Following the initial spin-up of the ensemble member vortices over the first 24 hours, the axisymmetric ensemble means are examined. The axisymmetric means are appropriate for this idealized study due to the lack of asymmetric forcing like vertical wind shear. The structure will be examined with 24 hour ensemble means to prevent the diurnal cycle from complicating the Fullrad analysis. Fig. 4.1 shows 24-h axisymmetric averages of the 10-cm radar reflectivity, potential temperature (θ), and secondary circulation for days 2, 3, and 4. The ensemble mean is shown in the middle panel plots in Fig. 4.1 (B, E, H) with the left (A, D, G) and right (C, F, I) panels of Fig. 4.1 showing the anomalies from the mean for the TT196 and TT202 experiments respectively. The ensemble means show the convective growth and very little tilt of the eyewall. The secondary circulation wind vectors indicate strong vertical motion in the eyewall with radial inflow below and a strong radial outflow around 13 km. On day 4, a weak layer of inflow beneath the outflow can be seen. Reduced static stability is found in the layer between 8-14 km which is quickly diminished by the eyewall convection. Isentropes descend in the eye as the warm core grows in strength. The radius of maximum winds (RMW) shows only small differences between the ensemble means but is at a small radius of ~30 km near the surface.

The differences between the structure of TT196 and TT202 are highlighted by the anomalies in Fig. 4.1. On day 2, the largest differences are seen in the potential temperature anomalies at the upper levels. The θ anomalies are the difference in the initial temperature profile that persists throughout the simulations. It is therefore expected that these θ anomalies will persist in all the experiments in the upper troposphere outside of the eyewall with some modifications due to the radiation schemes. Over

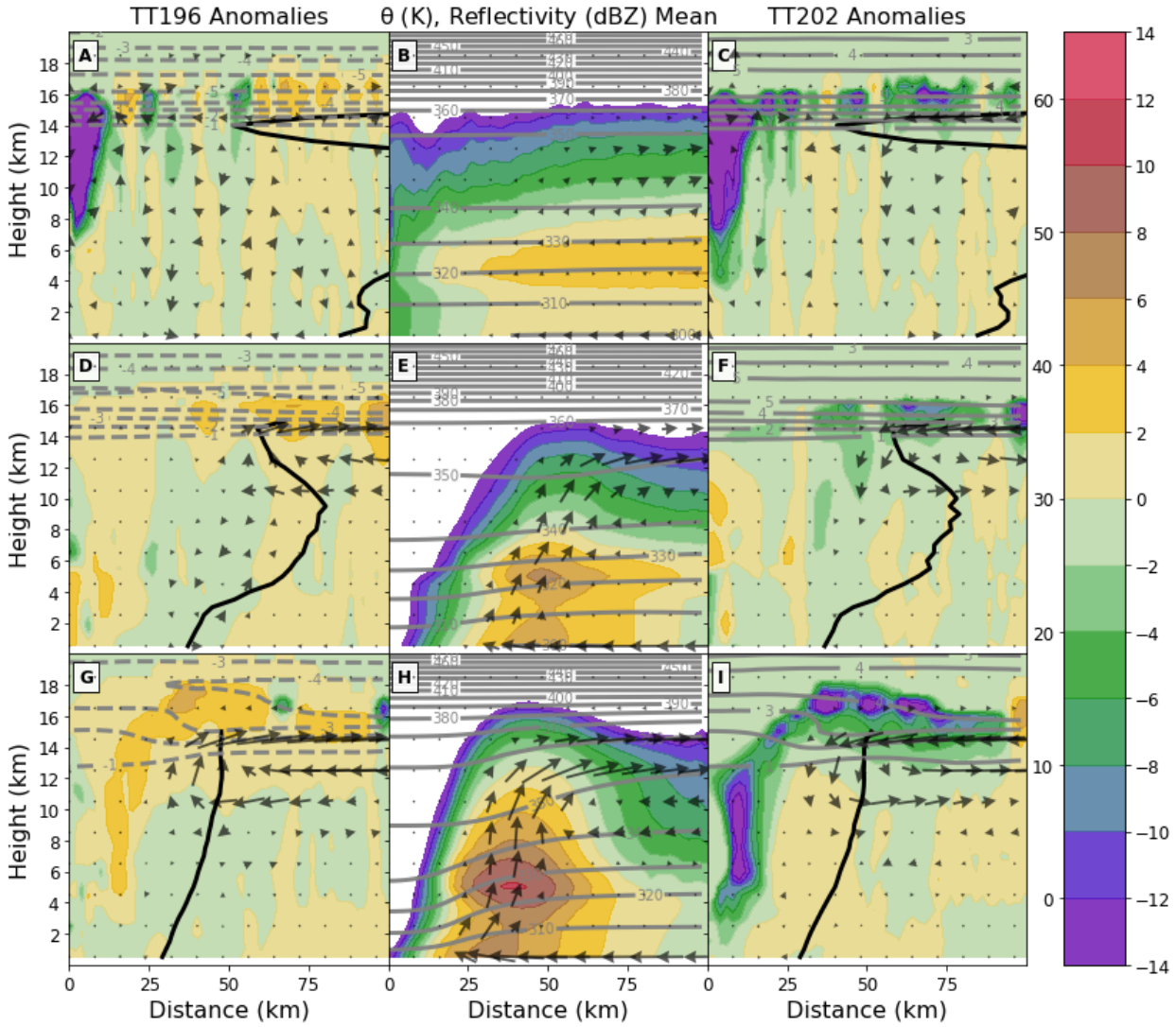

FIG. 4.1. Axisymmetric mean potential temperature (θ, contoured) and reflectivity (shaded) for Norad simulations between t=24-48h (A, B, C), t=48-72h (D, E, F), and t=72-96h (G, H, I). Middle panel plots (B, E, H) are the ensemble means with Îÿ contours every 10 K and reflectivity shaded every 5 dBZ with reflectivity below -5 dBZ whited out. Left paneled plots (A, D, G) show the anomalies of TT196 from the ensemble mean and right paneled plots (C, F, I) show the anomalies of TT202. The θ anomaly contour interval is 1 K and the zero line has been removed for clarity. Negative θ anomalies are dashed. Black line indicates RMW up to 15 km. Secondary circulation is denoted by wind vectors with magnitudes less than 1 m s^{-1} removed. The wind vectors have been increased by a factor of three in the vertical only.

time these θ anomalies decrease in magnitude over the eye as the warm core intensifies. Anomalies are also found in the reflectivity field with higher reflectivity found at the upper edge of the clouds in and above the eyewall in TT196 and reduced reflectivity in TT202. The reflectivity difference corresponds to a change in the storm top height where TT196 is taller and TT202 is shallower. Additionally, there

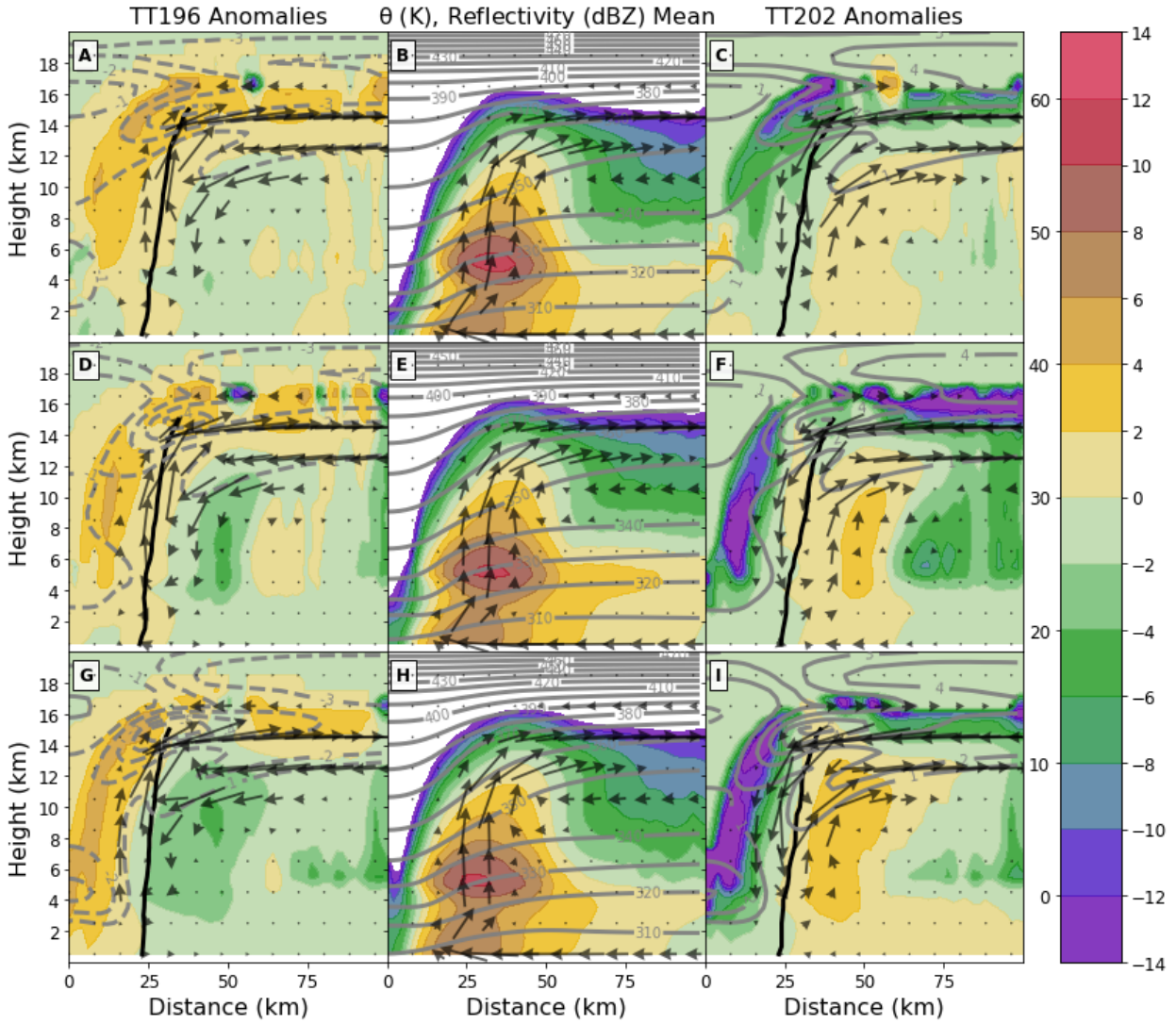

FIG. 4.2. Same as Fig. 4.1 but for different times between t=96-120h (A, B, C), t=120-144h (D, E, F), and t=144-168h (G, H, I).

are anomalies in the secondary circulation that develop as the TCs intensify. In TT196 it is shown that there is an increase in the outflow and an increase in the inflow located just below. In TT202 the opposite is present where the outflow is weakened and the inflow below is also weakened. The anomalous circulation occurs only at the upper levels and does not affect the circulation at the surface even as the TCs intensify. The confined location of the anomalies to the upper levels again corresponds to an increase in the height of the storm and the maximum outflow level.

Fig. 4.2 shows the mean and anomalous structures of the Norad simulations from days 5, 6, and 7. During this time all three ensemble means were intensifying slowly and were at nearly the same intensity. The ensemble means show that at each time the TCs had strong vertical motion in the near

vertical eyewall with a full tropospheric warm core at the center. Strong outflow with a layer of radial inflow both below and above is evident. The weak inflow above the outflow layer is occurring at the base of the CPT and is similar to the observations found by Duran and Molinari (2018) in Hurricane Patricia (2015). The strength of the outflow decreases radially outward and over time it seems that the depth of the outflow layer also decreases. Exceptionally high reflectivity is continuously found in the eyewall and highlights the compactness of the TCs without radiation.

The anomalies in Fig. 4.2 shows similar anomalies in the secondary circulation that occurred in the early time periods. These anomalies are confined to the upper levels with increased differences in the vertical motion around the eyewall. The anomalous circulation in the outflow again corresponds to an increase in the height of the outflow with the changes in the vertical motion inside the eyewall from a slight radial shift in the RMW. The reflectivity anomalies also highlight this radial shift in the eyewall and the increase in height of the TC with increased reflectivity at higher altitudes in TT196 compared to that of TT202. Shifting of the TC vortex from changes to upper-level temperatures can not however explain the anomalous potential temperatures in the eye. These anomalies show that the warm core of TT196 was weaker and did not extend as far downward as the warm core of TT202. Slow dynamically induced subsidence in the eye from eyewall convection in TT196 is advecting the lower θ anomalies downward, while the TT202 simulations are advecting the higher θ anomalies downwards. It is unclear however why the potential temperature anomalies reverse around 17 km in the eye. This small anomaly is not likely an artifact of the axisymmetric averaging as it grows in magnitude at the end of the simulation.

In summary, without the effects of radiation the height of the top of the storm is modified by the upper tropospheric temperatures. Associated with this change in height there are anomalies in reflectivity and changes to the secondary circulation at the upper levels. The change in height response to changes in upper tropospheric temperatures is expected and was noted by Wang et al. (2014); however, there were additional changes to the thermodynamics of the eye in the Norad simulations. Upper tropospheric temperatures caused θ anomalies in the warm core structure of the idealized TCs. It is unclear as to if the warm core anomalies contribute in any way to the intensities in the Norad experiment. It is generally recognized that the magnitude of the warm core increases with the intensity of a TC due to thermal wind and/or hydrostatic balance (Ohno et al. 2016); however, even though TT196 and TT202 had similar intensities, θ anomalies in the warm core were ~5 K different. The anomalies in the secondary circulation never manifest themselves at low levels to alter tangential winds. However,

as there are no changes to the maximum intensity of the TCs, increasing the height of the storm is not sufficient to increase the intensity of the storm.

4.2 Radiative Impacts

How radiation, together with upper tropospheric temperatures, change the structure of idealized TCs will now be diagnosed. Fig. 4.3 shows 24-h axisymmetric averages of the 10-cm radar reflectivity, potential temperature, and secondary circulation for days 2, 3, and 4 of the Fullrad experiments. Similar to Fig. 4.1, the ensemble mean is shown in the middle panel plots (B, E, H) with the left (A, D, G) and right (C, F, I) panels showing the anomalies from the mean for the TT196 and TT202 experiments. The effects of both shortwave and longwave radiation cause a broader storm compared to the Norad simulations with increased eyewall tilt. The ensemble means also show the development of a stronger warm core compared to the Norad simulations at both the lower and upper levels. The Fullrad and Norad ensemble means have otherwise similar structures.

The initial difference in upper tropospheric potential temperatures is evident and is similar in magnitude between TT196 and TT202. The potential temperature anomalies are subsequently modified above the eye of the incipient TC with a reduction in the anomaly magnitudes. The reduction in θ anomalies indicates that the TT196 upper-level warm core has warmed more than TT202's relative to the environment. Additionally the potential temperature anomalies are reduced compared to the Norad experiment due to shortwave heating. Along the inner edge and above the eyewall there are differences in reflectivity, with TT196 having increased dBZ values while TT202 has reduced values. The reflectivity anomalies primarily indicate that similar to the Norad simulations, the height of the TCs differ due to differences in upper tropospheric temperatures with increased ice at a higher level. Anomalies in the secondary circulation initially occur at the upper levels in the Fullrad simulations with a similar pattern as the Norad simulations; however, the anomalies spread downwards modifying the vertical motion throughout the eyewall. TT196 has stronger vertical motion throughout the eyewall within the RMW and stronger inflow near the surface while TT202 has weaker vertical motion within its RMW and weaker inflow. These anomalies are present at the upper levels due to the differences in upper tropospheric temperatures and changes to the height of the storm, before propagating downwards through cloud-radiative feedbacks.

The Fullrad experiments peak in intensity between t=96-120h and are shown in the top panels of Fig. 4.4. The ensemble means show a much broader storm in the Fullrad experiments compared to

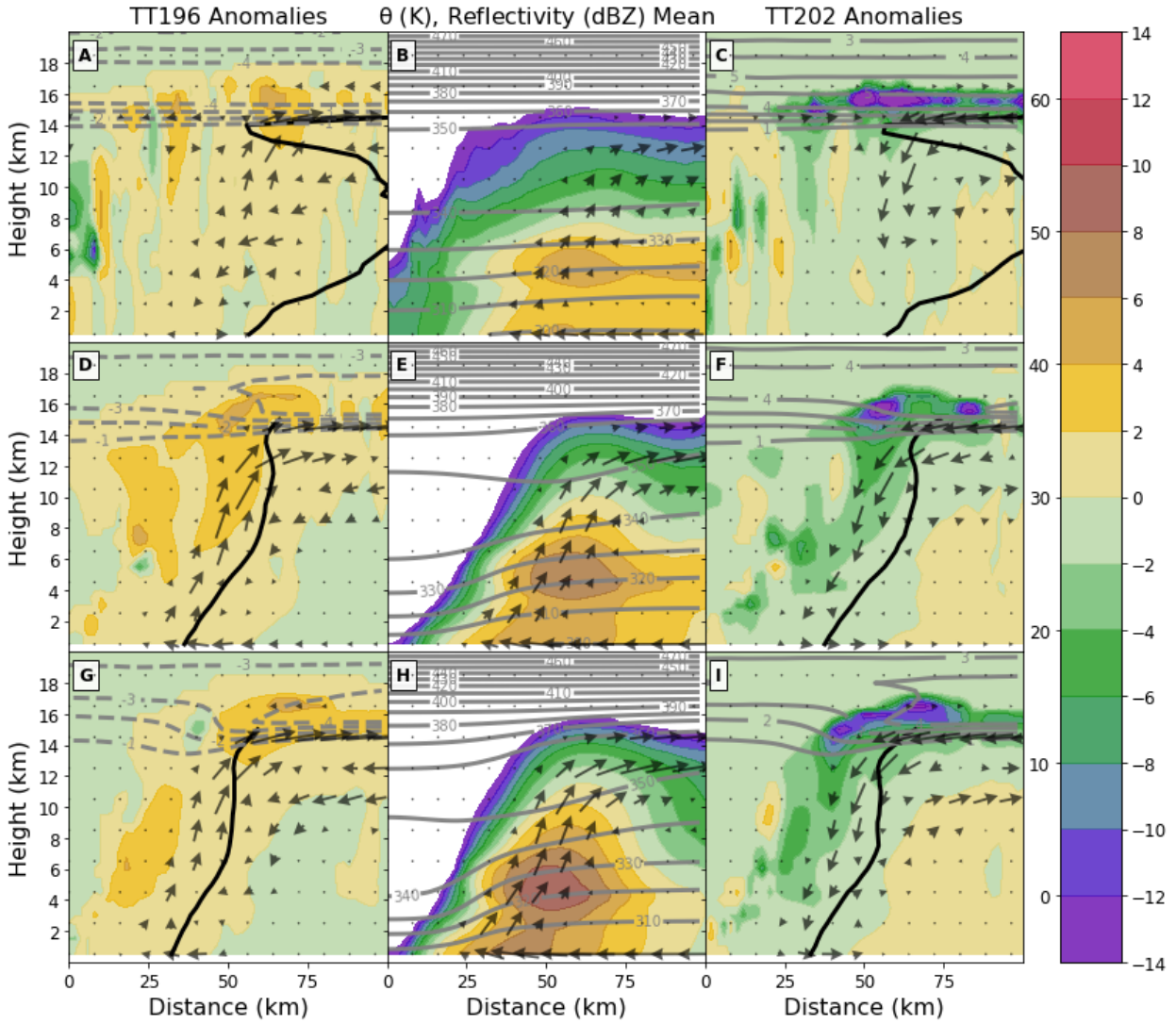

FIG. 4.3. Same as Fig. 4.1 but for Fullrad simulations.

that of the Norad with a more tilted eyewall. The outflow occurs throughout a deeper layer and does not have any inflow below or above the outflow jet which occurred in the Norad simulations. The θ contours in the eye are not as tightly packed indicating reduced static stability and an overall weaker warm core compared to that of the Norad. However, the primary eyewall is weakening from day 5 on and is evident by the reduced vertical motions in the eyewall and reduced reflectivity. The formation of a secondary eyewall occurs simultaneously with this weakening which is occurring outside of the domain shown.

Although the Fullrad experiments undergo an eyewall replacement cycle the secondary circulation anomalies in Fig. 4.4 are similar to that of the Norad simulations near its peak intensity. Both

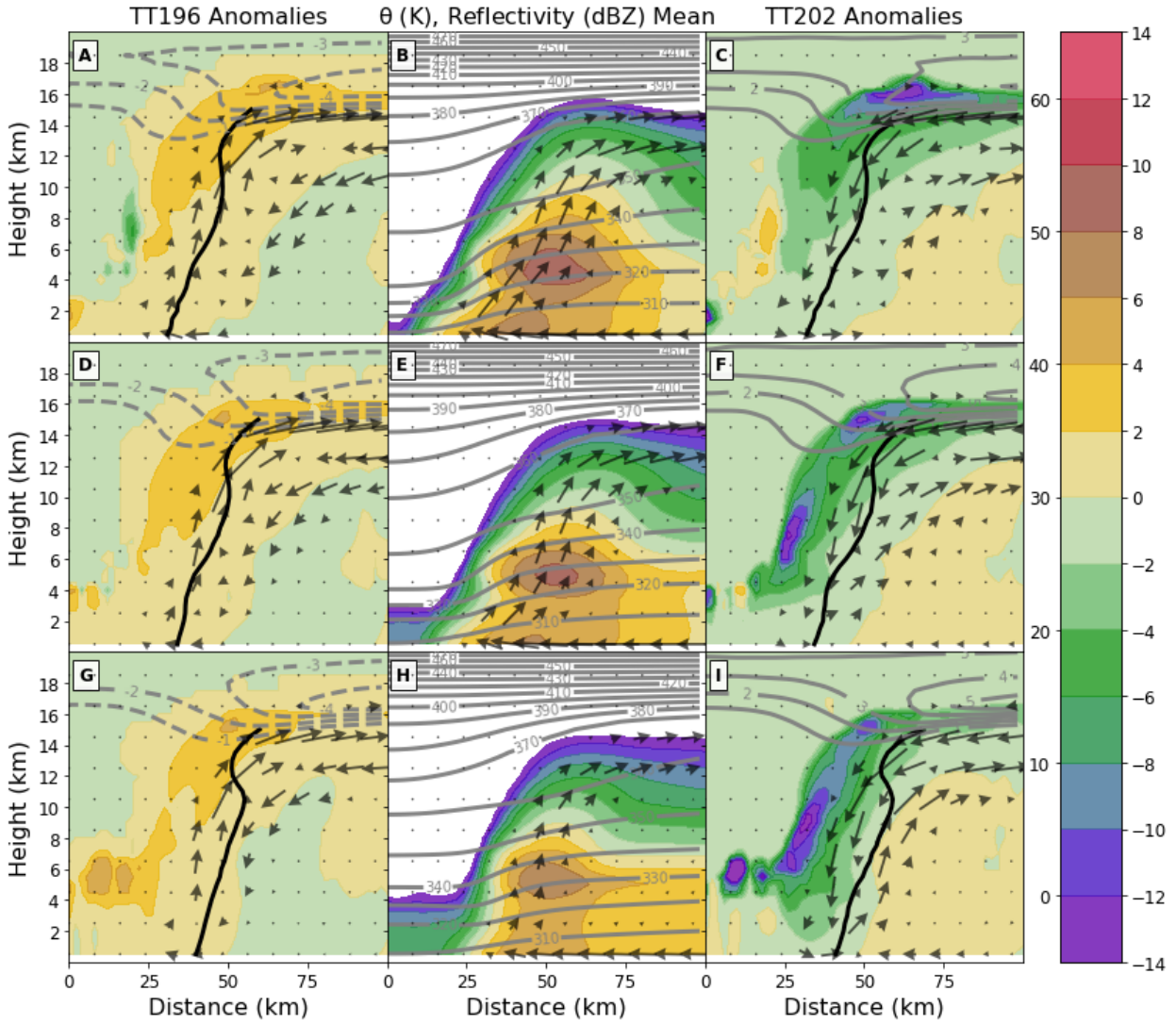

FIG. 4.4. Same as Fig. 4.3 but for different times between t=96-120h (A, B, C), t=120-144h (D, E, F), and t=144-168h (G, H, I).

have TT196 exhibiting the same toroidal motion in the outflow layer with enhanced outflow aloft and anomalous inflow just below that descends along the outer edge of the eyewall. The anomalous secondary circulation magnitude remains similar to the previous times indicating that the Fullrad anomalies may be a balanced response to the upper tropospheric temperatures. The most important difference between the Norad and Fullrad is that the secondary circulation anomalies in the Fullrad experiment extend throughout the vertical extent of the eyewall while the Norad anomalies do not. This means that the upper-level anomalies were able to spread downwards through feedbacks that modified the low level radial and tangential flow. There were also differences between the θ anomalies of the two experiments as the anomalies were not manifested into the warm core structure of the Fullrad

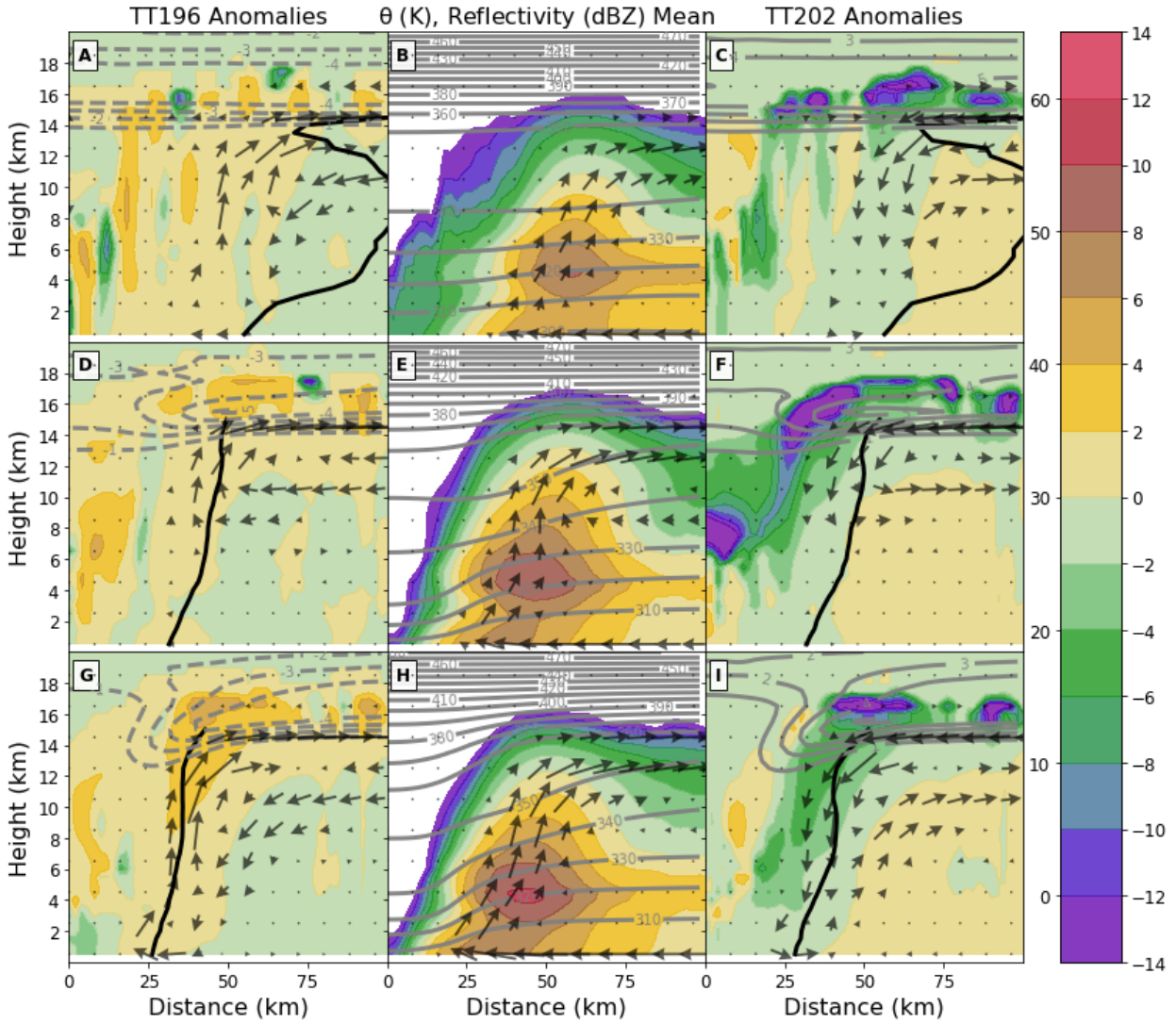

FIG. 4.5. Same as Fig. 4.1 but for the Nightonly experiment.

eye as expected. The warm core of each Fullrad TC was similar despite differences in magnitude of the vertical motion in the eyewall. The absence of the upper-level radial inflow in the Fullrad experiment may have reduced the isentropic downglide shown in the Norad simulations of modified upper tropospheric θ values into the eye. The formation of the secondary eyewall and reduction of the overall intensity of the warm core may also contribute to the lack of anomalous warming in the eye.

Fig. 4.5 shows the same axisymmetric mean profiles as Fig. 4.1 but for the Nightonly simulations. The Nightonly ensemble means are similar to the Fullrad simulations from t=24-48h with differences growing with time. The reflectivity core in the eyewall of the Nightonly simulations is more comparable to the reflectivity core in the Norad simulations which exceeds 55 dBZ after 72 hours. The RMW

in the anomaly panels are smaller and more vertically stacked compared to the Fullrad RMWs and are also smaller than those of the Norad simulations. This indicates that the shortwave radiation is important for changing the vortex size since the Nightonly and Norad ensembles have more similar RMWs. This supports the idea that shortwave warming may be supplemental to longwave warming in the anvil which past studies (Bu et al. 2014; Fovell et al. 2016) have found to be the primary mechanism in expanding TC wind fields. The isentropes in the eye have also declined in height throughout the troposphere demonstrating a full tropospheric warm core at a relatively early time. The secondary circulation evolves similar to the Fullrad except for a layer of inflow developing just below the outflow on day 3 which was similar to the upper-level radial inflow found in the Norad simulations. The overall structure of the Nightonly simulations are consistent with the Fullrad and Norad simulations with the primary differences in the means being the RMW.

Although differences in the ensemble means at the early times exist between the Fullrad and Nightonly experiments, the anomalies are qualitatively similar. TT202 has overall lower reflectivity values above and along the inner edge of the eyewall. In the potential temperature fields, the initial anomalies above the eye are minimized indicating that the warm cores of TT196 and TT202 are becoming more similar. However, relative to the environments in which the storms were modeled, more upper-level eye warming must be occurring in TT196. Above the eyewall the greatest θ anomalies have collapsed to a smaller area around the cloud top with some anomalies being advected downward along the inner edge of the eyewall. Similar to the Fullrad and Norad simulations, anomalies in the secondary circulation are found at the upper levels. This anomalous toroidal circulation causes stronger outflow in TT196 and a weaker outflow in TT202. With time, secondary circulation anomalies manifest themselves at low-levels causing stronger upwards motion in TT196 and weaker vertical motion in TT202. The radial dipole in vertical motion along the RMW in the Nightonly simulations also corresponds to a slight radial shift of the eyewall which is seen at the later times of each experiment. This radial shift in the RMW is small yet present in each of the experiments near peak intensity. This could be an artifact of the azimuthal averaging, or it could indicate that the upper tropospheric temperatures play a role in modulating the size of the TC vortex.

Over time through cloud-radiative feedbacks the anomalous secondary circulation strengthens in the Nightonly simulations. Fig. 4.6 highlights both the mean and anomalies for the Nightonly simulations just prior to and at peak intensity. The θ anomalies in the eye of the Nightonly simulations are significantly different from that of both the Fullrad and Norad simulations. In the TT196 simulations

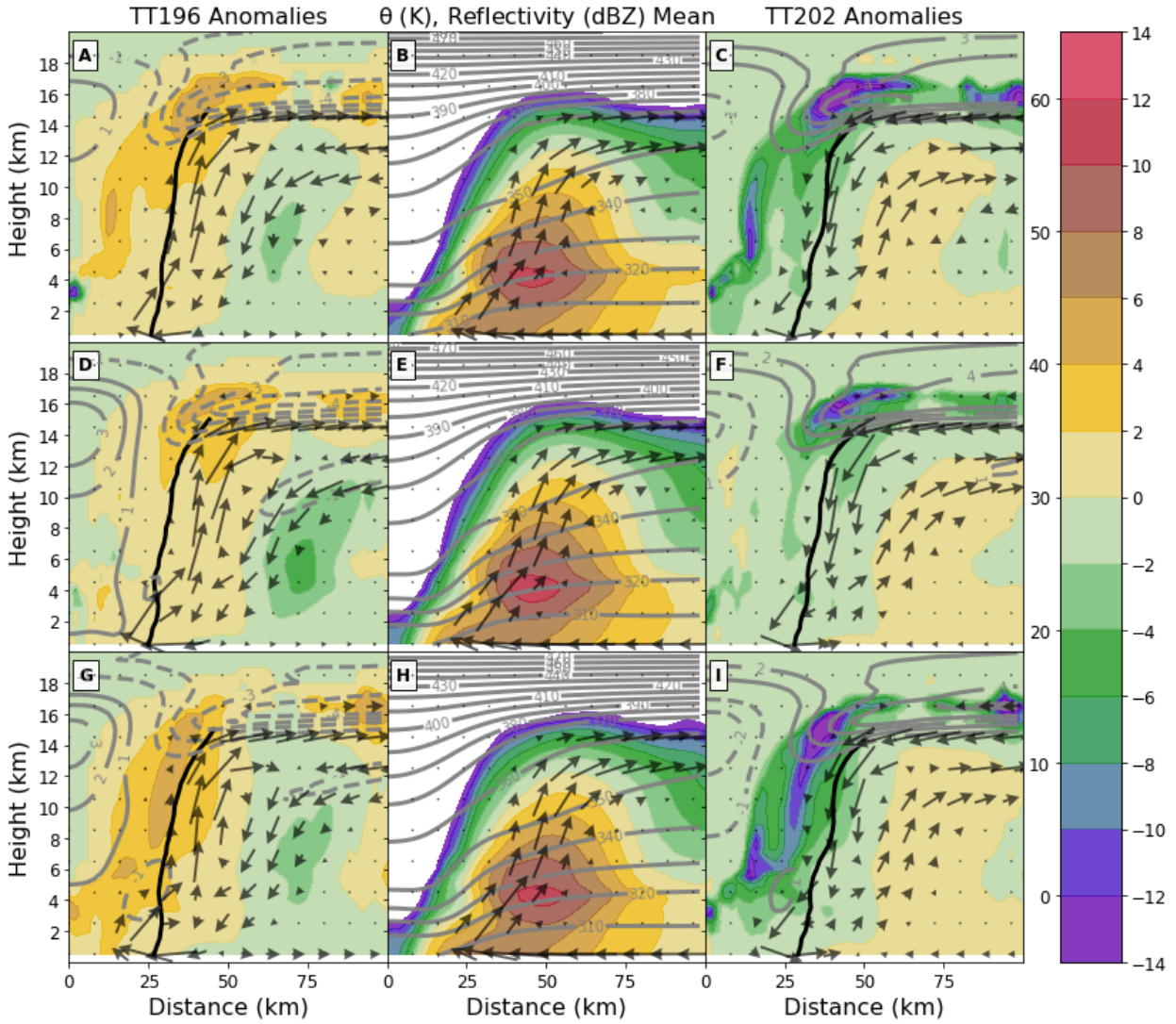

FIG. 4.6. Same as Fig. 4.5 but for different times between t=96-120h (A, B, C), t=120-144h (D, E, F), and t=144-168h (G, H, I).

the warm core potential temperature becomes enhanced while the warm core in TT202 is reduced, particularly at the upper levels. This is opposite of the Norad simulations but what is expected because TT196 is a more intense TC than TT202. The warm core of the Nightonly simulation is stronger than the Fullrad and Norad likely due to the effects of longwave radiation and enhanced vertical motion in the eyewall. The cause of the warm core differences between TT196 and TT202 may be explained simply by the fact that TT196 is a more intense TC than TT202 (Ohno et al. 2016). However, as will be shown in the following section, an increase in radiative cooling rates may have also increased the subsidence in the eye.

4.3 Mass Transport by Secondary Circulation

The previous discussion of the structure of the axisymmetrized simulations showed anomalous circulations that we will now examine quantitatively in detail. Vertical and radial mass fluxes are calculated since differences in density arise from the initial temperature variations and the radiation schemes over time. Fig. 4.7 shows the positive vertical mass flux over the 48 hours prior to peak intensity of each experiment and the anomalies from from the means. The vertical mass flux in the Nightonly simulations were stronger compared to that of the Fullrad which were in turn stronger than that of the Norad. The lower vertical mass flux in the Norad simulations is a product of the small storm size. The stronger low-level mass flux in the Nightonly simulations supports the results of Navarro and Hakim (2016) in which increased low level diabatic heating in the eyewall was found to occur indirectly from longwave radiation. Anomalies in the vertical mass flux show very similar patterns between each of the ensembles indicating that the effect of upper tropospheric temperatures is to affect the upper-level mass flux by changing the storm top height. Colder upper tropospheric temperatures yielded more upper-level mass flux with the opposite occurring due to warmer temperatures. The anomaly is consistently weaker for the Fullrad simulation compared to the Nightonly simulation and maximizes at a slightly lower altitude. These differences in upper-level mass flux are due to stability differences owing to sharper lapse rates. The reduced vertical mass fluxes in the Fullrad simulations are attributed to the competing effects of destabilization by longwave cooling and stabilization by shortwave heating. The mean vertical mass flux profiles are dependent on the radiation schemes and the anomalies are dependent on the upper tropospheric temperatures. Since strong upper-level mass flux anomalies are found in both the Nightonly and Norad experiments, we are unable to tease out the contributions to upper-level mass flux anomalies from radiation and the effects of changing the height of the TCs.

The evolution of the radial mass flux and the associated anomalies within each experiment are important for understanding the net effect of the upper tropospheric temperatures on the maximum sustained wind variation of the simulations. Fig. 4.8 shows the mean radial mass flux with time for each experiment. First focusing on the means, it is shown that the radial inflow is much stronger in the Nightonly simulations compared to both the Fullrad and Norad experiments and persists much longer. The Fullrad simulations actually have the weakest outflow which weakens near the end of the simulation as the primary eyewall decays and secondary eyewall forms. The Nightonly and Norad experiments have similar outflow magnitudes with the Norad outflow becoming stronger on average at

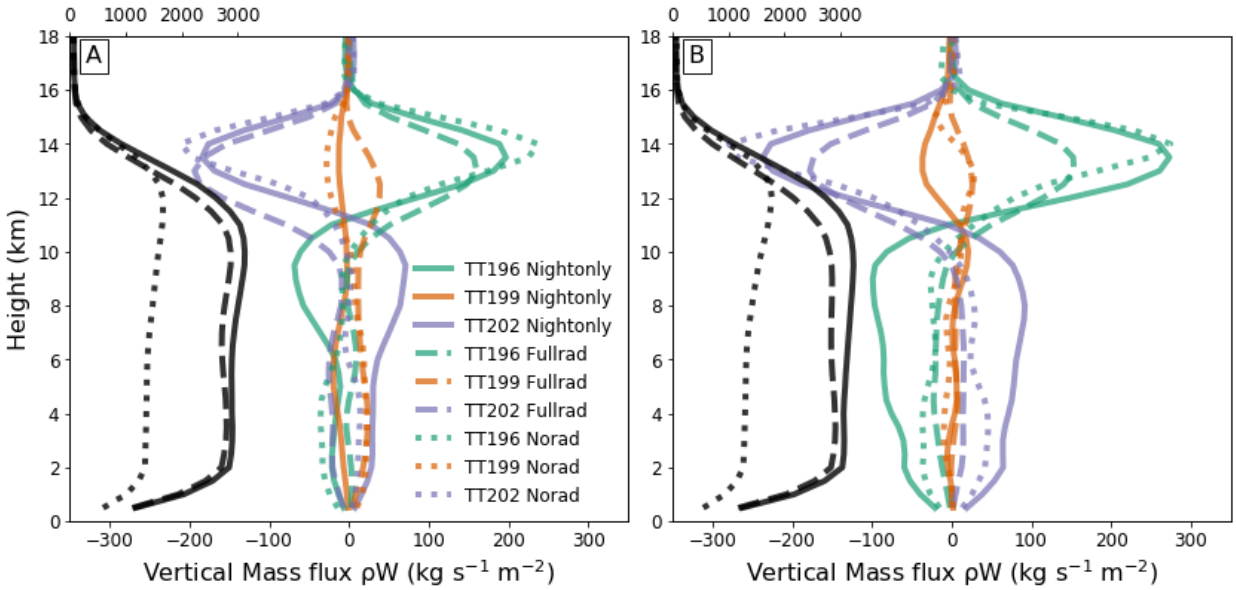

FIG. 4.7. Total upwards vertical mass flux (kg s^{-1} m^{-2}) means (black) and anomalies between r=0-100 km for the 48-24 hours prior to peak intensity (A) and 24 hours prior to peak intensity (B). Profiles taken from ensemble means of the Nightonly (solid), Fullrad (dashed), and Norad (dotted) simulations. The ensemble means (anomalies) are plotted according to the top (bottom) abscissa.

the later time periods. The anomalies in radial mass flux are considerably different for the distinct radiation schemes. In the Nightonly experiment, TT196 has an overall stronger outflow than TT202. In the Fullrad there are weak differences between TT196 and TT202. The Norad simulations have a dipole in which TT196 has stronger outflow but compensates with anomalous inflow below it while the dipole reverses in TT202. This again indicates that in the Norad simulation there is a shift in height of the storm while in the Nightonly and Fullrad there is a change in the strength of the outflow and a shift in height.

In order to get a better understanding of how radiation and upper tropospheric temperatures altered the mass transport by the secondary circulation, the radial mass flux is integrated. Fig. 4.9 shows the integrated radial mass flux for two different boxes extending from r=0-100 km using Simpson's rule. The dashed line is the radial mass flux from z=0-3 km and represents the strength of the inflow. The solid line is integrated from z=8-16 km and represents the strength of the radial outward mass transport or outflow. Comparing the area between the outflow and inflow lines gives a sense of the strength of the secondary circulation and total mass transported by the TC. The ensemble means show that the Nightonly had both stronger inflow and outflow. The Fullrad simulation had stronger inflow and

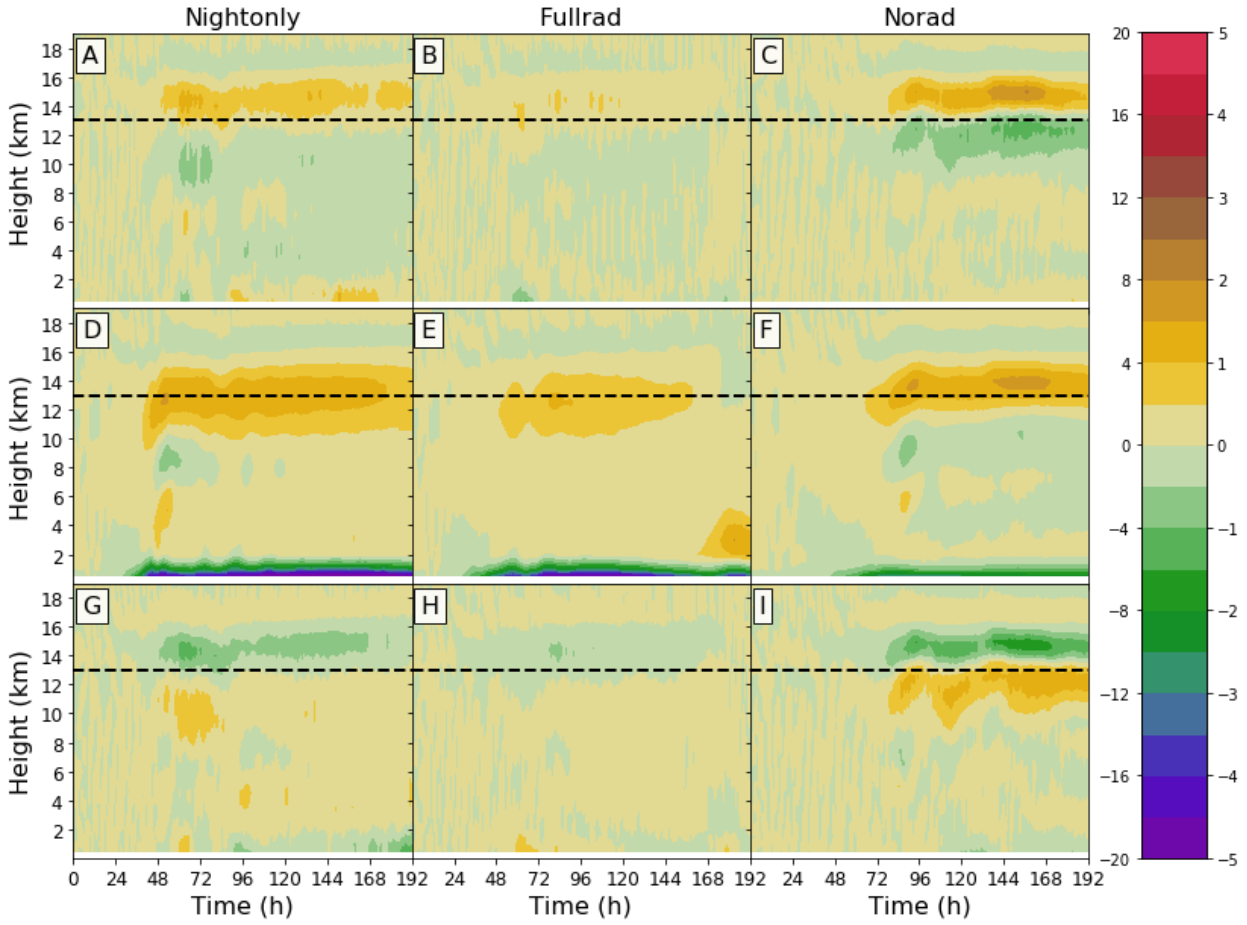

FIG. 4.8. Axisymmetric mean from r=40-100 km mass weighted radial wind (kg s^{-1} m^{-2}) Hovmöllers for Nightonly (D), Fullrad (E), and Norad (F) simulations. Upper paneled plots (A, B, C) show the anomalies of TT196 from the ensemble mean and lower paneled plots (G, H, I) show the anomalies of TT202. The ensemble means (anomalies) employ values on the left (right) side of the colorbar. The dashed black line at z=13 km allows for a better comparison of the anomalies and the means.

outflow compared to the Norad simulations before the formation of the secondary eyewall. By analyzing the anomalies, it is shown that TT196 had both a stronger outflow and inflow in the Nightonly and Fullrad experiments while TT202 had a weaker inflow and outflow over a majority of the simulations. However in the Norad experiment, the anomalies were much weaker in magnitude and near zero for a majority of the simulation. The Norad simulations between t=120-144h had stronger outflow in TT196 compared to TT202, but this was compensated for by a weaker inflow in TT196 compared to TT202. This confirms the hypothesis that radiation is responsible for modifying the mass transport of the secondary circulation that leads to stronger storms with colder upper tropospheric temperatures.

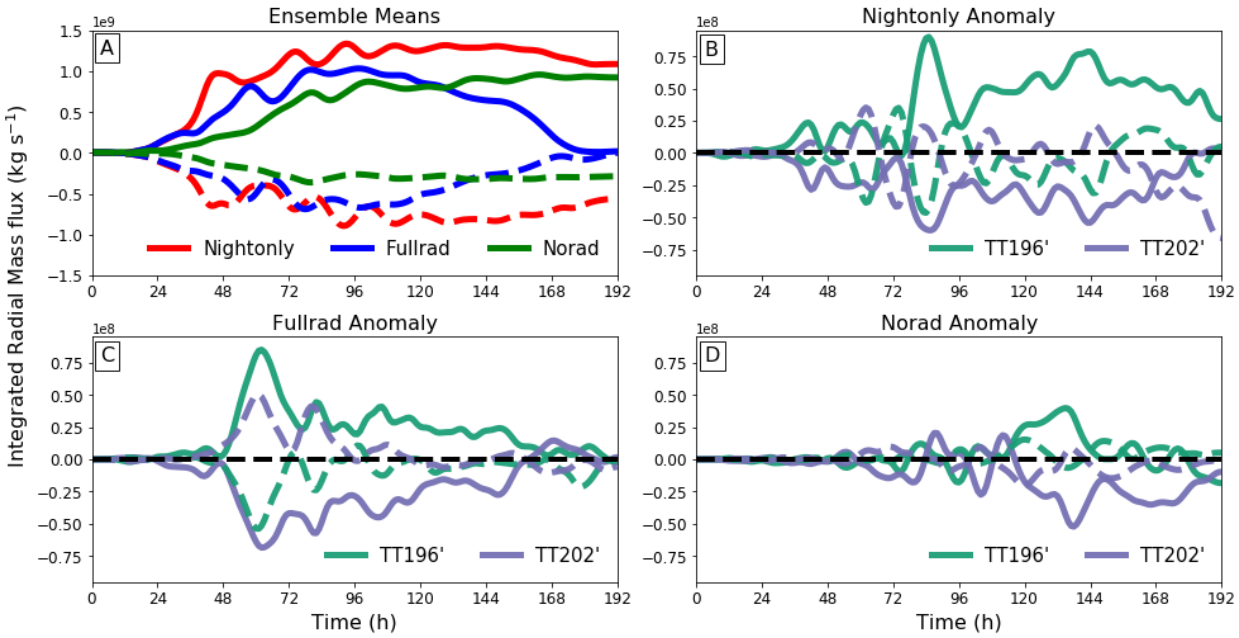

FIG. 4.9. Integrated radial mass flux from r=0-100 km for the ensemble axisymmetric means (A). Only the Nightonly (B), Fullrad (C), and Norad (D) anomalies for TT196 and TT202 are shown for clarity since TT199 is nearly the mean. The solid lines are integrals from z=8-16 km and dashed lines are the integrals from z=0-3 km. The black dashed line is the zero anomaly line. Smoothed using 10 iterations of a 1-2-1 filter with weights of .25, .5, and .25 respectively.

Radiation has been shown to affect the secondary circulation in the Fullrad and Nightonly simulations to modify the maximum intensity of TCs. The radiative tendencies are now analyzed to diagnose the mechanism by which radiation affects the secondary circulations in these experiments. Contrasts in the radiation tendencies will help to explain differences between TT196, TT199, and TT202. Wang et al. (2014) noticed the upward shift in the outflow jet but their simulations would not be able to resolve cloud feedbacks between the radiation and convection in RCE. Fig. 4.10 shows the net radiative tendencies for the Fullrad simulations with the radial flow contoured. At the early time period (t=24-48h) there exists a layer of radiative cooling with weak outflow below and weak 5 m s^{-1} inflow in the boundary layer. There is already a subtle anomaly in the net radiative tendencies with TT196 having a stronger cooling tendency and TT202 having a weaker cooling tendency at cloud top. Over the next 24 hours the ensemble mean outflow and inflow both intensify as previously shown. The mean longwave cooling increases in area with a larger area of shortwave and longwave warming below. The radiative anomalies also strengthen as the TC strengthens with a dipole developing where in TT196 there is a cooling anomaly over a warming anomaly and vice versa for TT202. The radial flow dipole anomaly is due in part to the cloud tops of the TCs being at different levels and develops in the location of the

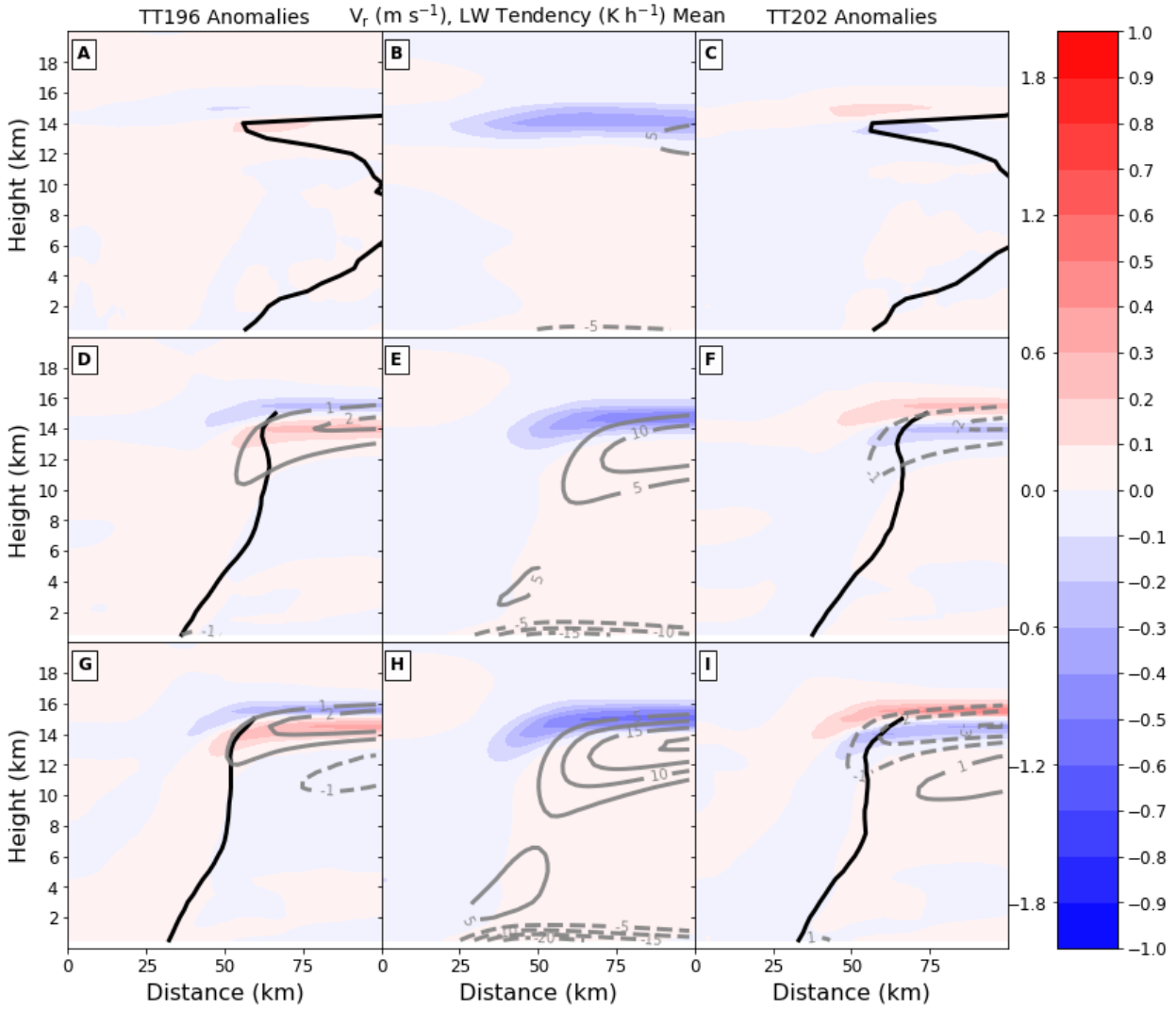

FIG. 4.10. Axisymmetric mean radial wind (contoured) and net radiative tendencies (shaded) for Fullrad simulations between t=24-48h (A, B, C), t=48-72h (D, E, F), and t=72-96h (G, H, I). Middle panel plots (B, E, H) are the ensemble means with radial wind contour intervals of 5 m s^{-1}. Left paneled plots (A, D, G) show the anomalies of TT196 from the ensemble mean and right paneled plots (C, F, I) show the anomalies of TT202. The radial wind contour interval is 1 m s^{-1} with the zero line removed from each plot for clarity. Negative radial winds are dashed. Black line indicates the RMW up to 15 km.

vertical gradient in radiative tendencies. The inflow and outflow dipole produced by an upper-level heat source is consistent with the results of Navarro et al. (2017) using a time varying equation for the circumferential component of vorticity (Willoughby 2009) similar to the Eliassen equation (Eliassen 1952). In the t=72-96h ensemble mean the secondary circulation of the TCs continue to intensify in addition to the cooling tendency directly attributed to the longwave radiation. There is an enhancement in the radiative tendency means with time but the radiative anomalies and the outflow anomalies

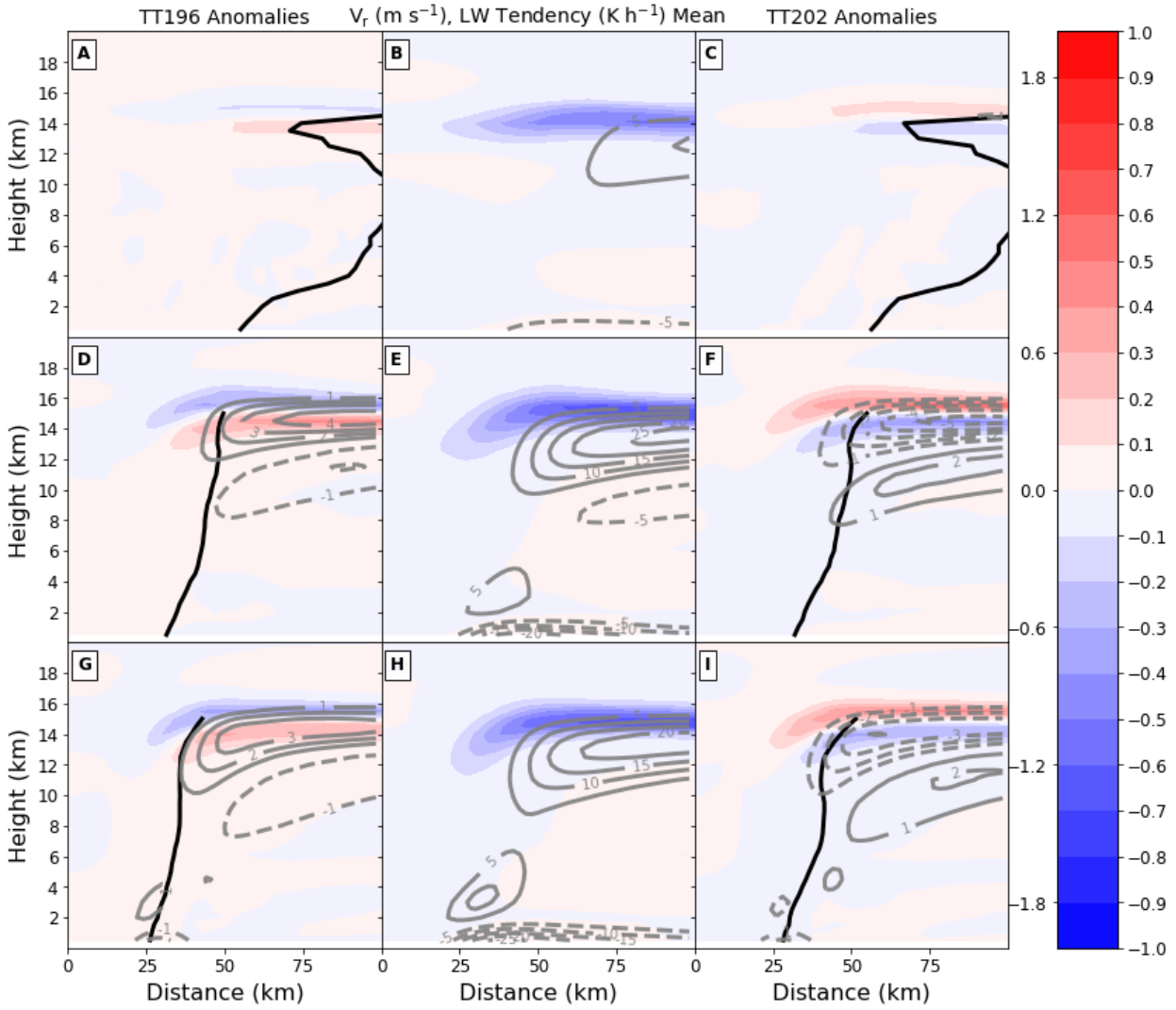

FIG. 4.11. Same as 4.10 but for Nightonly simulations.

remain consistent. Through to the end of the Fullrad simulations, the TT196 and TT202 anomalies in the outflow remain close to 2 m s^{-1} (Fig. 4.4) with constant 24 hour average radiative tendency anomalies.

In the Nightonly experiments the radiative tendencies are due only to longwave radiation. Since shortwave heating is no longer offsetting longwave cooling, the magnitude of radiative cooling in Fig. 4.11 is noticeably larger than in Fig. 4.10. The t=24-48h ensemble means have stronger inflow and outflow over a larger area compared to the Fullrad simulations and a slight cooling tendency throughout instead of a warming. Over the next 24 hours the radial flow intensifies rapidly with 20 m s^{-1} inflow and 25 m s^{-1} outflow. In the anomalies at this time there is the same dipole in radiative tendencies as in the Fullrad simulations but the magnitude and areal coverage is larger. There is a stronger response in

the outflow with TT196 having approximately 6 m s^{-1} stronger outflow than TT202. It is important to note that as was previously shown, the radial wind anomalies occurred in the upper troposphere and have not yet manifested themselves at the low levels. The t=72-96h ensemble mean again shows strong longwave cooling occurring above the eyewall extending into the eye. The ensemble mean outflow has slightly weakened but the upper-level inflow has also been reduced and the inflow in the boundary layer has increased. Similarly the outflow anomaly magnitudes have also been slightly reduced; however, they remain much stronger than the Fullrad anomalies. Anomalies have now begun to manifest themselves at low levels with TT196 having a slightly enhanced inflow that grows in magnitude over the following hours (Fig. 4.6).

The ensembles showed that both upper tropospheric temperatures and radiation played an important role in changing the dynamic and thermodynamic structure of TCs. It has been shown that when radiation is included, colder upper tropospheric temperatures have resulted in deeper TCs with more reflectivity and vertical mass flux at upper levels while warmer upper tropospheric temperatures have yielded the opposite. This causes heating anomalies to develop in the radiative tendencies which have affected the secondary circulation as expected from the balanced response described by the Eliassen equation. By causing a heating anomaly below a cooling anomaly in the longwave tendencies of TT196 and an overall stronger cooling maximum, a stronger secondary circulation arises with forced outflow above and inflow below. This suggests that by increasing the height of the vortex with the inclusion of radiative anomalies the TC intensity should increase. This mechanism for intensification explains why the Nightonly simulations had stronger heating anomalies, stronger anomalies in the secondary circulation, and overall stronger TCs compared to the Fullrad simulations. This hypothesis is supported by the work of Navarro et al. (2017) where upper-level radiative forcing caused by shortwave heating produced local overturning circulations. These upper-level heating anomalies in Navarro et al. (2017) however did not contribute to larger tangential winds at the surface likely due to the periodicity of the forcing and its concentrated location outside of the RMW. The heating anomalies in these idealized TCs extended a large distance in the upper troposphere nearly 300 km long at later times in the extensive anvil of the Nightonly simulations. The expansive area of heating anomalies could contribute to a larger enhancement as seen by Navarro and Hakim (2016) and will be the subject of future work.

Although it is hypothesized that the upper-level radiative heating anomalies are primarily responsible for the variability in intensity from the Nightonly and Fullrad simulations, it may not be the only

mechanism for understanding the intensity differences between the Fullrad and Nightonly simulations. It is thought that cloud-free radiative cooling could also be a potential mechanism for explaining the intensity differences between the Fullrad and the Nightonly simulations (Gray and Jacobson 1977). In the Nightonly simulations the enhanced cloud free environmental subsidence driven by more longwave cooling could force stronger inflow into the TC. Due to the short time scale of this study and the large anvil that develops, this mechanism may play a part in the initial intensity differences between the simulations but not the later time periods and as such may be complementary. No substantial differences were present in the outer core radiative cooling rates over the 24 hours means. The reduced intensity difference in the Fullrad simulations is consistent with the work by Schmetz and Beniston (1986) in which solar radiation reduces the strength of cloud secondary circulations by offsetting cloud-top infrared cooling. This is likely a contributing factor as to why the Fullrad simulations did not develop the same warm core potential temperature anomalies as the Nightonly simulation. The effects of radiation and the radiative heating anomalies are important in determining the TC intensity.

CHAPTER 5

VARIABILITY DUE TO LONGWAVE RADIATION

The simulations with longwave only radiation exhibited much stronger variability caused by the random moisture perturbations compared to the Fullrad and Norad simulations. It is not immediately clear why such variability exists and only in the Nightonly simulations. In order to address this sensitivity the two strongest and two weakest ensemble members from the Nightonly TT196, TT199, and

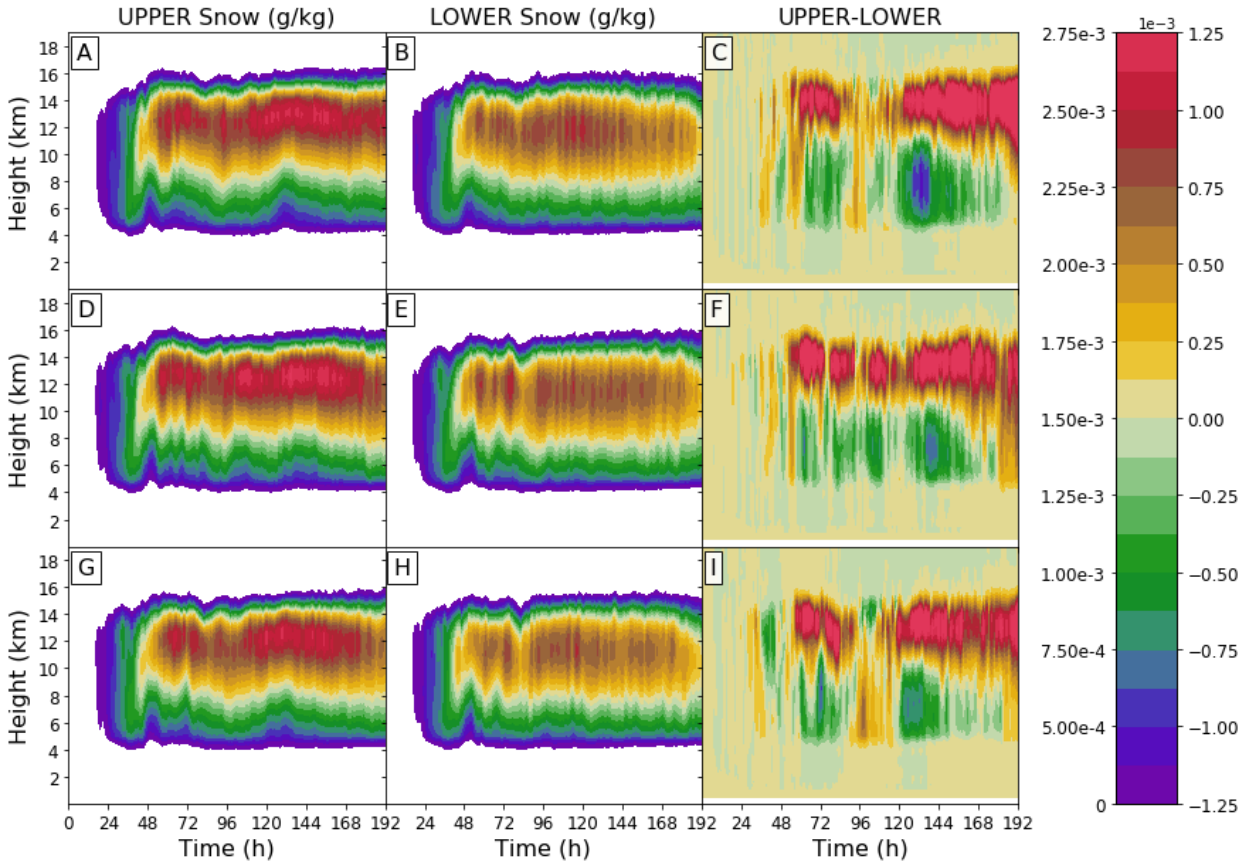

FIG. 5.1. Axisymmetric mean from r=40-100 km of snow mixing ratio (g kg^{-1}) Hovmöllers for the Upper and Lower bounds of the Nightonly simulations. Each row corresponds to a different experiment of TT196 (A, B, C), TT199 (D, E, F), and TT202 (G, H, I). The left panel plots (A, D, G) are an average of the two strongest TCs from the Nightonly simulations. The middle paneled plots (B, E, H) are an average of the two weakest Nightonly TCs and the right paneled plots (C, F, I) are the difference of the weakest from the strongest TCs. The means (differences) employ values on the left (right) side of the colorbar. Snow mixing ratio means below zero are whited out.

TT202 will be composited. This will give an upper and lower bound for each experiment to then use to diagnose the sensitivity to longwave radiation caused by the moisture perturbations.

Differences in the RMW may help to explain some of the variance in the Nightonly simulations but major differences occur in the height of the TCs. Fig. 5.1 shows Hovmöllers of the snow mixing ratio for the average of the two strongest (UPPER), two weakest (LOWER), and the difference for TT196, TT199, and TT202 of the Nightonly simulations. The UPPER TCs have larger amounts of snow mixing ratio through the early time periods indicating enhanced moisture in the inner core region. The random moisture perturbation caused differences of 0.5-1.5% in the relative humidities in the inner core between the two strongest and two weakest TCs. It is due to this anomaly in relative humidity that outflow anomalies subsequently develop at cloud top with stronger TCs having increased upper-level ice concentrations while weaker TCs have less. The anomalies in snow mixing ratio corresponding to both an increase in magnitude and height of the maximums for stronger storms. The differences in upper-level clouds would then interact with the radiative tendencies and feedback to influence the intensity.

Fig. 5.2 now shows the radiative tendencies focused on the upper levels. The overall evolution of the longwave tendencies are similar in the UPPER TCs and LOWER TCs however the magnitudes and heights are different. As expected based on the amount of upper-level clouds, the UPPER TCs exhibited stronger cooling rates that occurred at an elevated height. As previously shown in the structural differences between the Fullrad and Nightonly simulations, this change in height will then increase the height of the radiative tendencies and cause a positive heating anomaly with a cooling anomaly above. This will then induce an enhancement in the secondary circulation which is shown in Fig. 5.3. The average of the two strongest TCs has a much stronger radial outflow compared to the average of the two weakest TCs for a majority of the simulations. There is also an anomalous radial inflow below the outflow layer which arises due to the previously shown height differences.

Changes to the height of the radiative anomalies explain the variability of the intensity within the Nightonly simulations. The sensitivity of the longwave simulations to the small boundary layer moisture perturbations arises due to the moisture perturbations ability to impact the amount of upper-level clouds. This calls into question the predictability of TC intensities using only longwave radiation if such a small perturbation can cause 15 m s^{-1} differences in maximum wind speeds. This sensitivity will therefore be also dependent on the microphysics and radiation schemes employed by the model. The model sensitivity to the complex interactions between the microphysics and radiation schemes will be the topic of further study.

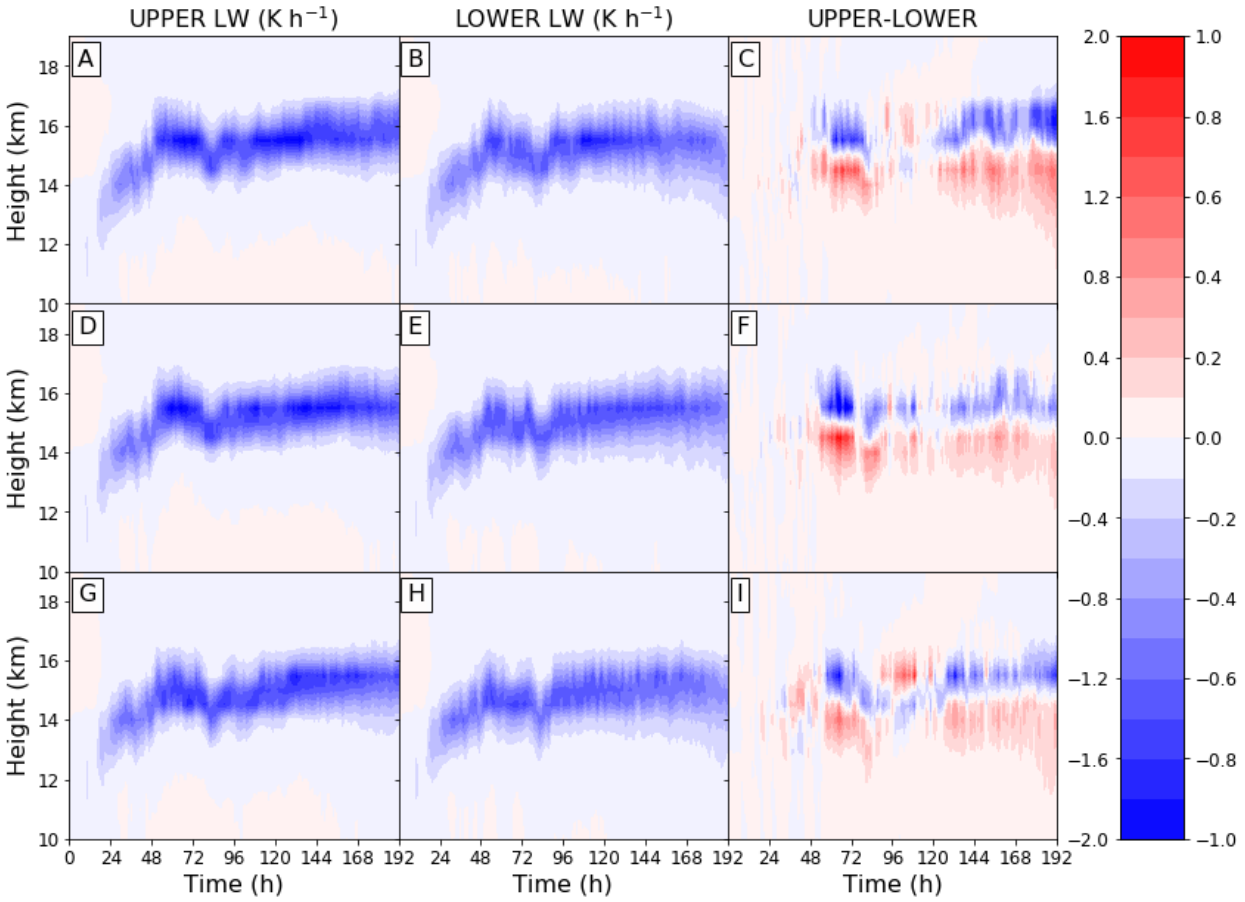

FIG. 5.2. Axisymmetric mean from r=40-100 km of longwave radiative tendencies (K h^{-1}) Hovmöllers for the Upper and Lower bounds of the Nightonly simulations. Each row corresponds to a different experiment of TT196 (A, B, C), TT199 (D, E, F), and TT202 (G, H, I). The left panel plots (A, D, G) are an average of the two strongest TCs from the Nightonly simulations. The middle paneled plots (B, E, H) are an average of the two weakest Nightonly TCs and the right paneled plots (C, F, I) are the difference of the weakest from the strongest TCs. The means (differences) employ values on the left (right) side of the colorbar.

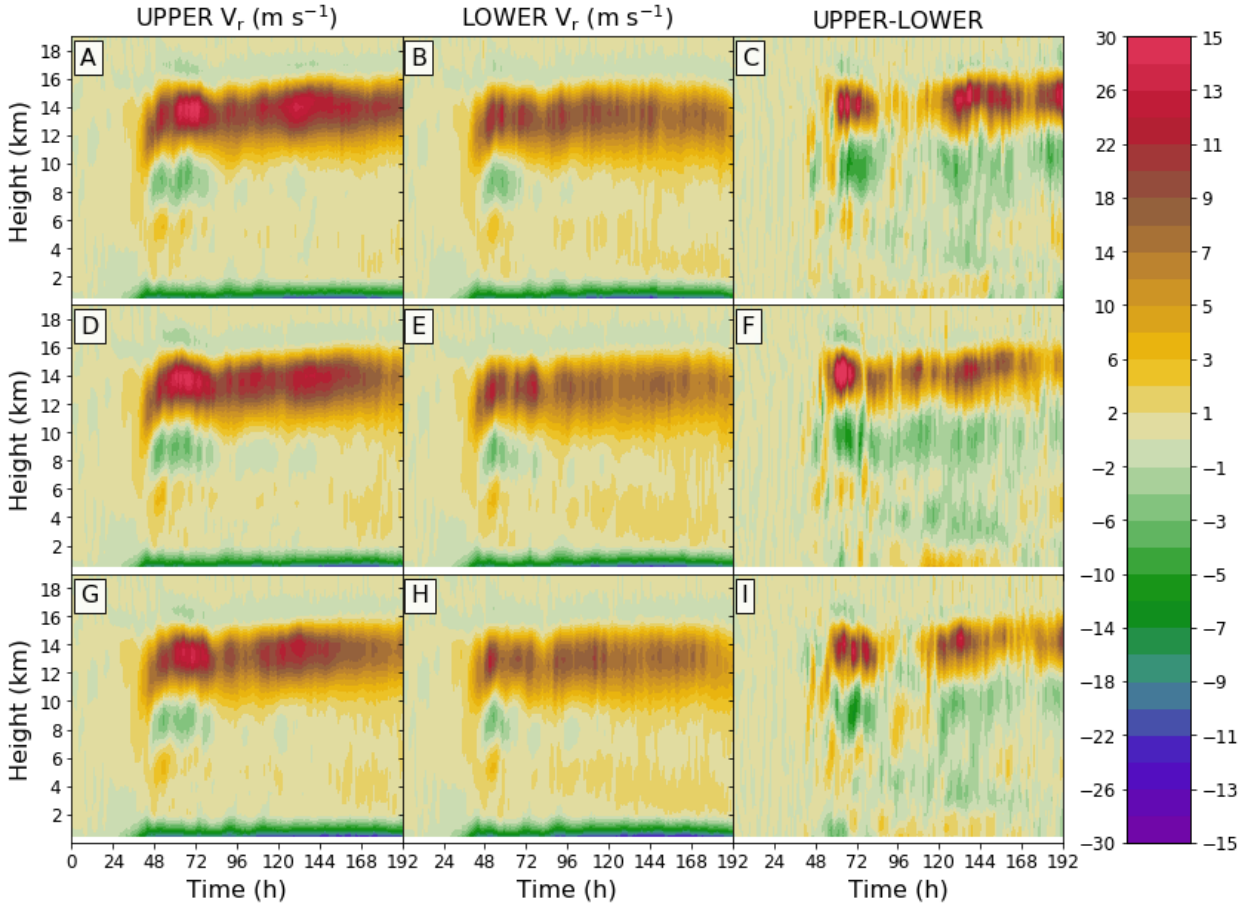

FIG. 5.3. Axisymmetric mean from r=40-100 km of radial wind (m s^{-1}) Hovmöllers for the Upper and Lower bounds of the Nightonly simulations. Each row corresponds to a different experiment of TT196 (A, B, C), TT199 (D, E, F), and TT202 (G, H, I). The left panel plots (A, D, G) are an average of the two strongest TCs from the Nightonly simulations. The middle paneled plots (B, E, H) are an average of the two weakest Nightonly TCs and the right paneled plots (C, F, I) are the difference of the weakest from the strongest TCs. The means (differences) employ values on the left (right) side of the colorbar.

CHAPTER 6

RADIATION IN THE CARNOT MODEL

As shown by the preceding simulations and past studies (e.g. Nolan 2007), radiation is not a necessary requirement in order to successfully simulate strong TCs; however, radiation is required to fully understand the closed Carnot heat engine model for TCs. The Carnot model assumes that radiation is essentially negligible everywhere except during the isothermal compression leg. Both the adiabatic expansion and isothermal compression legs of the Carnot cycle are both controlled directly by the temperatures of the upper troposphere. By changing the depth of the TC by decreasing the upper tropospheric temperatures, the adiabatic expansion leg is implicitly modified, but the isothermal leg where radiative effects may be more important will be primarily discussed.

During the adiabatic expansion leg air erupting from the boundary layer at the RMW is brought upwards and radially outwards along a constant angular momentum surface at constant moist entropy to large radii. The temperature that this parcel reaches is the outflow temperature which has been defined using different methods over the years (e.g. Emanuel 1986, 2012). The outflow temperature will not be quantified in each simulation but instead refer the reader back to Figs 4.1-4.6 to highlight that TT196 indeed had the coldest outflow temperature while TT202 had the warmest. At this outflow temperature longwave radiation and subsidence warming are assumed to balance each other during the isothermal compression leg as air descends at large radii (Emanuel 1986, 1997, 2003). OLR acts as the heat sink while subsidence warming counteracts the radiative tendency. Thus it seems that the longwave radiation is important for maintaining the Carnot cycle while shortwave heating is not explicitly included in the theory. Emanuel (1989) found that when radiative cooling was omitted from their experiment the maximum winds attained only 85% of their control experiment and that longwave cooling was necessary for a quasi-steady state to be reached. Since longwave radiation is necessary to understand the Carnot model this motivates the in depth analysis of the Nightonly simulations.

The larger the temperature difference between the heat source and sink the greater the thermodynamic efficiency. In this experiment, by changing the upper tropospheric temperatures the heat sink and the thermodynamic efficiency have been modified. There exists a 1% difference in the thermodynamic efficiency as described by the Carnot efficiency between each of TT196, TT199, and TT202. The actual values however, are sensitive to the outflow temperature definition. The thermodynamic efficiency does not explain the lack of intensity difference in the Norad experiments and is similar to

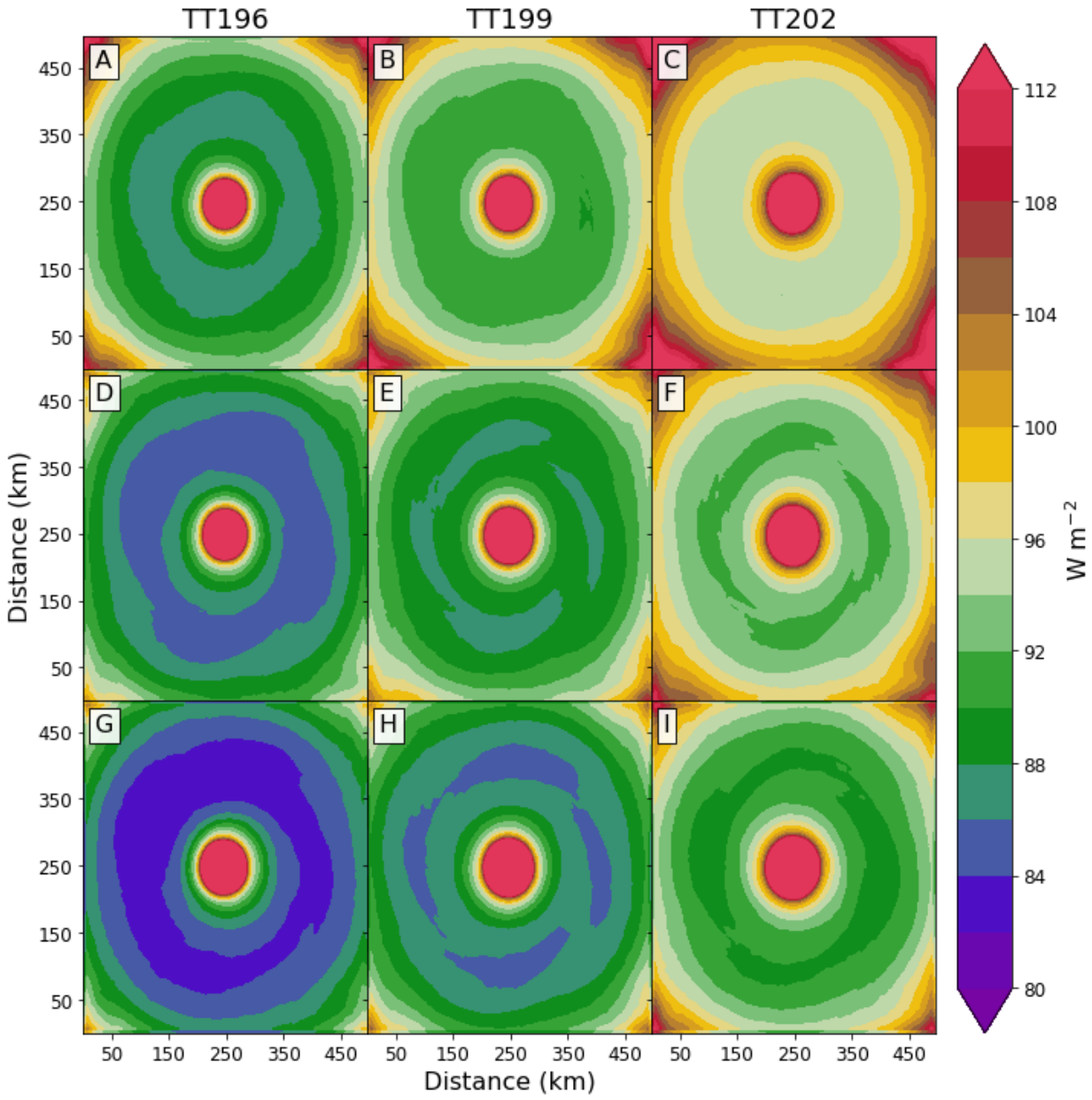

FIG. 6.1. OLR for Nightonly simulations between t=96-120h (A, B, C), t=120-144h (D, E, F), and t=144-168h (G, H, I). Left panel plots (A, D, G) are from the TT196 ensemble mean, middle panel plots (B, E, H) from the TT199 mean, and right panel plots (C, F, I) are from the TT202 ensemble mean.

the accounts of past studies that showed convective instability is a poor predictor of PI (Rotunno and Emanuel 1987; Emanuel 1989; Camp and Montgomery 2001). Additionally, in the Nightonly experiments, the 1% difference cannot explain the large intensity differences. How radiation was modified between experiments was therefore analyzed. Fig. 6.1 shows three different 24h averages of OLR for

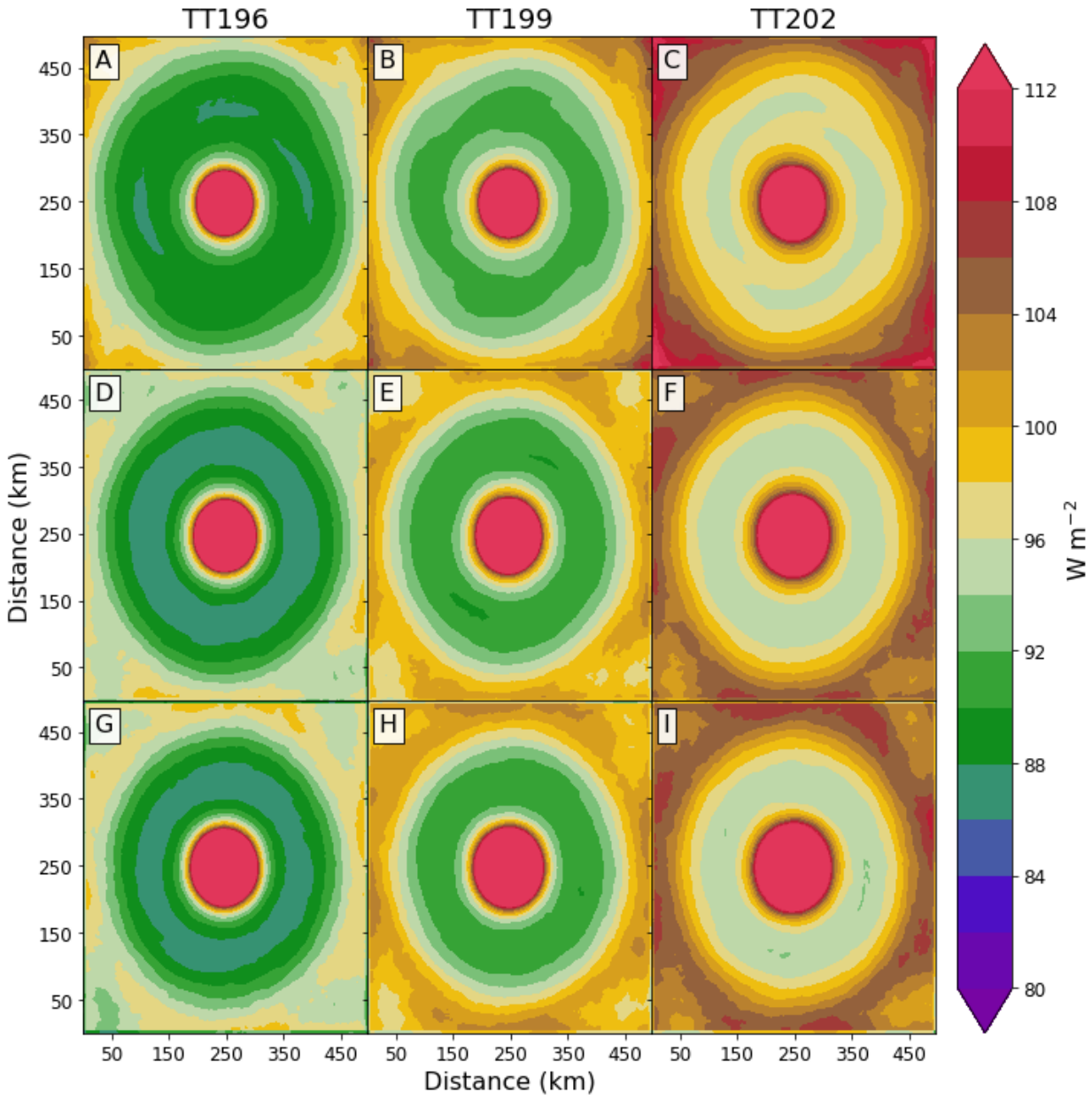

FIG. 6.2. Same as Fig. 6.1 but for the Fullrad experiments.

each of the Nightonly experiments. Over all time periods TT196 had colder upper tropospheric temperatures so the amount of OLR was reduced while TT202 which had warmer upper tropospheric temperatures had more OLR. This also occurred in the Fullrad simulations shown in Fig. 6.2 confirming that the OLR differences were primarily due to the colder upper tropospheric temperatures. Compared to the Nightonly TCs the Fullrad TCs emitted more OLR meaning that the storm top height is lower but the heat sink is increased. In both cases the weaker TT202 is emitting more radiation and therefore has a stronger heat sink than the more intense TT196 simulations. This is counterintuitive because a

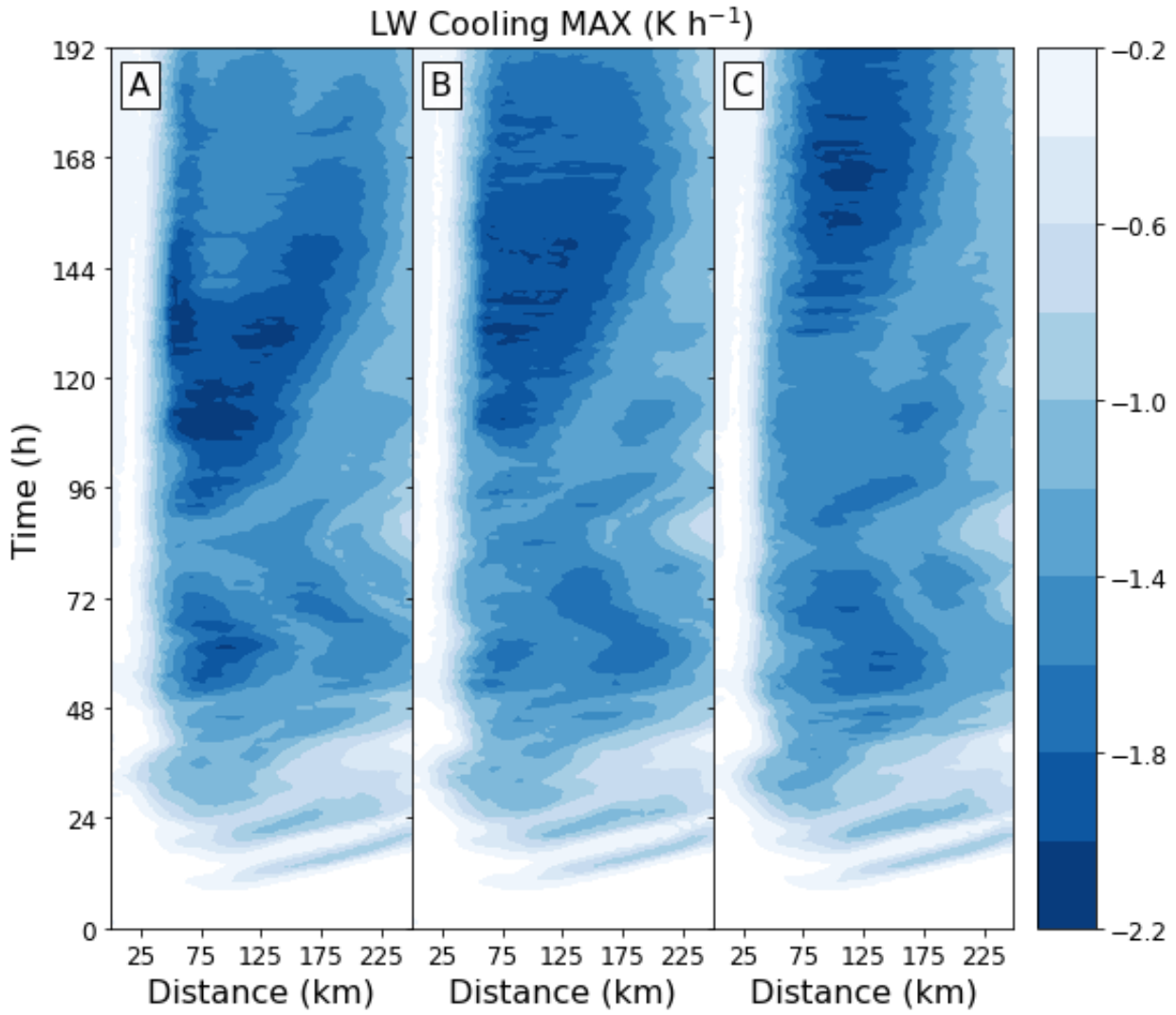

FIG. 6.3. Minimum longwave tendencies (K h^{-1}) Hovmöller from Nightonly axisymmetric ensemble mean for TT196 (A), TT199 (B), and TT202 (C).

stronger heat sink found in the Fullrad TCs compared to the Nightonly TCs and in TT202 versus TT196 would be preferred for stronger TCs such that the amount of work available to the Carnot heat engine would be larger.

Fig. 6.3 shows a Hovmöller of the minimum longwave tendencies (i.e. the maximum cooling) for the Nightonly simulations ensembles. The longwave cooling rates were maximized at different times due to the differences in upper tropospheric temperatures. The timing of the longwave cooling maximums are associated with the time of peak intensities of each experiment which correlates to the previously shown time lag. While Fig. 6.1 showed that TT196 had less OLR, locally TT196 had larger longwave cooling rates near cloud top at those times. These enhanced cooling rates likely played a large

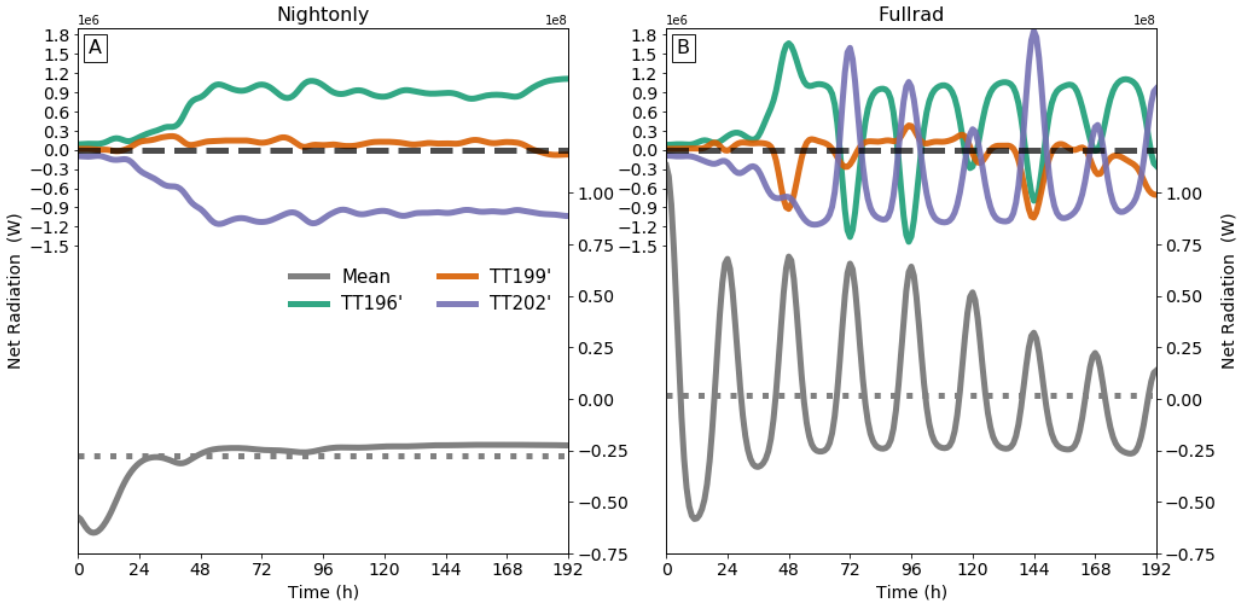

FIG. 6.4. Integrated net radiation over the innermost domain for the Nightonly (A) and Fullrad (B) ensembles. Anomalies are plotted on the left ordinate for each experiment and the ensemble mean (solid gray) is plotted according to the right ordinate. Negative (Positive) mean values indicate a net loss (gain) of radiation by the system. Gray dotted lines are the time averaged ensemble mean values and the black dashed line is where the anomalies are zero. Smoothed using 10 iterations of a 1-2-1 filter with weights of .25, .5, and .25 respectively.

role in enhancing the local buoyancy which supported the stronger vertical mass flux at upper levels shown previously in Fig. 4.7. In an integrated sense the inner domain of TT196 is actually cooling less than TT199 and TT202. Fig. 6.4 shows the integrated net radiation for both the Nightonly and Fullrad experiments. In the Nightonly experiments there is less integrated OLR in TT196 and more in TT202. In the Fullrad simulations there is less OLR at night in TT196 versus TT202 and less shortwave heating during the day in TT196 versus TT202. If the average net radiation is examined, it was nearly zero indicating that the effects of both radiation schemes offset each other on in an integrated sense. The reduction in OLR means that less heat can be extracted from the system although there is locally stronger radiative tendencies associated with radiative flux divergence. Because the TCs are deeper in the TT196, increased ice concentrations, the overall temperature profile, and sharper lapse rates allows for the enhanced cooling tendencies and reduced OLR.

In the isothermal compression leg, the cooling by emission of radiation is supposed to nearly balance the subsidence warming. The OLR was modified by the environmental temperatures such that the heat sink of the stronger TCs were less than that of the weaker hurricanes. Since locally stronger cooling rates were found in the stronger storms at cloud top, this implies that for balance to occur in

the isothermal leg weaker subsidence must occur for stronger TCs. However, by the closed TC Carnot model this should yield a weaker TC as parcels would subsequently be integrated downwards along a lower angular momentum surface. Even if subsidence warming does not completely balance with radiative cooling as shown by Hakim (2011) using an axisymmetric cloud resolving model, reducing longwave cooling should yield a weaker TC. It is therefore suggested that cloud-radiative feedbacks need to be considered as they play an important but complicating role in the system. Diagnosing each of these feedbacks is outside of the scope of this study as multiple mechanisms may play an important role at various times but remains an important area for future research (Tang and Zhang 2016).

It is hypothesized that the mechanism by which PI is sensitive to upper tropospheric temperatures is due to the cloud-radiative feedbacks. If only the effects of upper tropospheric temperature differences on TCs were considered, it would be expected to see deeper convection in the eyewall with anomalous upper-level mass flux (Fig. 4.7). However, it is likely the cloud-radiative feedbacks from longwave radiation due to differences in lapse rates that act to modify the PI. Xu and Randall (1995) found that on short time scales longwave cooling destabilizes the upper cloud layer by enhancing turbulent motion before enhancing cloud-scale motions on longer time scales. Small scale turbulence from longwave radiation could act to set the thermal stratification of the outflow which could modulate the intensity of TCs (Emanuel 2012). A more complete analysis of cloud-radiative feedbacks within intense TCs and the stratification of the outflow will be the topic of future study.

The heat source for hurricanes in the Carnot model is the gain of moist entropy from wind induced sensible and latent heat fluxes from the ocean. It has already been shown that radiation plays an important part in modifying the secondary circulation of TCs; however we have not considered feedbacks from stronger winds inducing stronger surface fluxes. The enhancement of surface fluxes would allow the TC to gain more energy resulting in a stronger storm even though in this study only the upper level thermal structure and the radiation schemes have been adjusted. Fig. 6.5 shows the evolution with time of surface enthalpy fluxes for the Nightonly and Fullrad experiments integrated over the innermost domain. The purpose of Fig. 6.5 is to show that no differences have been found in the surface enthalpy fluxes between TT1996, TT199, or TT202 for either experiment. The lack of differences confirms that changes to surface fluxes do not explain the modeled differences in maximum wind speeds found in this study.

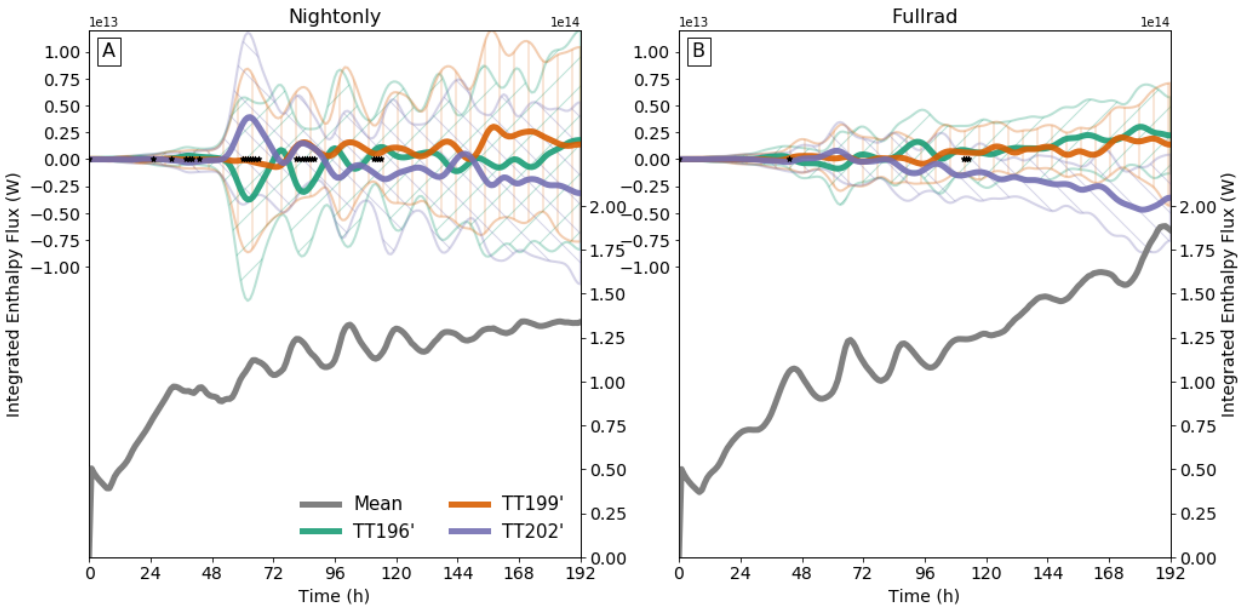

FIG. 6.5. Integrated enthalpy flux at the surface over the innermost domain for the Nightonly (A) and Fullrad (B) ensembles. Anomalies are plotted on the left ordinate for each experiment with hatched areas being ± standard deviation. The ensemble mean (gray) is plotted according to the right ordinate. Black points indicate occurrences where TT196 and TT202 are statistically significant at the 95% confidence level using a two-sided T-test. Smoothed using 10 iterations of a 1-2-1 filter with weights of .25, .5, and .25 respectively.

CHAPTER 7

CONCLUSIONS

In this study high-resolution simulations of idealized hurricanes were analyzed to gain a better understanding of how changing tropopause temperatures affect the potential intensity. A possible mechanism by which upper tropospheric temperature profiles modify both intensity and structure has been identified and the influence of radiation on modifying upper tropospheric temperatures on weather time scales has been assessed. By using ensembles, sensitivities to stochastic differences in convection have been addressed, but this study is still limited by the employment of only a single microphysics and radiation scheme. However, it is expected that the results of this study will qualitatively hold true for similar radiation and microphysics schemes.

It is important to note that PI in this framework (Emanuel 1986, 1988, 1997) assumes that TCs are in a state of radiative or statistical equilibrium of which the simulations in this study were not. Similar to the RCE experiments of Wang et al. (2014) and Ramsay (2013), colder upper tropospheric temperatures yielded stronger TCs but only when radiation was included. Therefore it can be stated that despite the time scale of only eight days, PI theory can qualitatively be used to identify changes to TC intensity from changing environmental thermodynamics. However, when radiation was neglected, the changes in upper tropospheric temperatures were not consistent with the PI theory. The effects of upper tropospheric temperatures on maximum intensity however is strongly dependent on the radiation scheme even in an idealized framework. The PI relationship appears to be linear using the three temperature profiles for the Fullrad simulations and possibly for the Nightonly simulations which is consistent with the RCE simulations of Ramsay (2013) and Wang et al. (2014). The same relationship cannot be determined for the Norad simulations. The Nightonly simulations were sensitive to the small moisture perturbations while the Fullrad and Norad simulations were less so. The boundary layer moisture perturbations influenced the height of the TCs which then intensified at different rates due to radiative heating anomalies. The Fullrad simulations were similar to the coarse simulations by Schmetz and Beniston (1986) of which the incorporation of shortwave radiation resulted in reduced instability in the convective layer leading to weaker interactions between clouds, radiation, and the mesoscale fields.

The upper tropospheric temperatures controlled the amount of upper-level vertical mass flux, ice species aloft, and caused changes to the height of the TCs on average. The depth of the TC is fundamentally related to the upper tropospheric temperatures as temperature declines with height until reaching

the tropopause. Although this creates more available convective energy it was shown by Rotunno and Emanuel (1987) and the preceding Norad simulations to play little to no role in the maximum intensity. The balanced response in the secondary circulation described by the Eliassen equation arises from the upper troposphere radiative cooling/heating anomalies. The magnitude of these anomalies and the corresponding effect on PI is controlled by the radiation and cloud-radiative feedbacks which are dependent on the temperature structure of the upper troposphere. The location of this heating relative to the RMW and its radial extent may also be important and therefore suggest that the diurnal cycle of intensities in a TC may be modulated by the extent of its cloud cover. It can be speculated that the larger cloud extant, area of radiative cooling, and subsequent response from the Eliassen equation at cloud top may explain why the signal of cyclical pulses in the infrared cloud field found by Dunion et al. (2014) were stronger in mature TCs where the cirrus shield is more developed.

Reduced outgoing longwave radiation because of a colder tropical tropopause layer means that from a Carnot engine perspective, the radiative heat sink is actually reduced in stronger storms. This suggests that as the TC height increases, the radiative fluxes must decrease which should create an inherent limit on the TC max intensity in the Carnot model. Cloud-radiative feedbacks are important for our understanding of PI but are not accounted for in the current Carnot model. The radiative feedbacks are important because the PI relationship to upper tropospheric temperatures in this study is not consistent with theory without the effects of radiation. The upper tropospheric lapse rates are also an important factor because they modify and are modified by the radiative tendencies on short time scales. Although the focus of this study was on the upper levels, the effects of radiation on the boundary layer inflow and height may also be important and is considered a topic of further research.

These results suggest that changes to the cold point tropopause are important for understanding and forecasting the intensity of TCs on short time scales. However, this work does not consider the impacts of phenomenon such as the quasi-biennial oscillation (QBO) or synoptic scale influences. The easterly phase of the QBO can cause anomalously cool temperatures in the upper troposphere and encourage the development of deep convection (Nie and Sobel 2015). Further study is warranted to fully understand the role of upper tropospheric temperatures in non-idealized hurricanes.

REFERENCES

Avila, L., 2017: Tropical storm Ophelia discussion number 10. [Available online at : `https://www.nhc.noaa.gov/archive/2017/al17/al172017.discus.010.shtml?`].

Bell, M. M. and M. T. Montgomery, 2008: Observed structure, evolution, and potential intensity of category five Hurricane Isabel (2003) from 12-14 September. *Mon. Wea. Rev.*, **136**, 2023–2046.

Bell, M. M., M. T. Montgomery, and K. A. Emanuel, 2012: Air-sea enthalpy and momentum exchange at major hurricane wind speeds observed during CBLAST. *J. Atmos. Sci.*, **69**, 3197–3222, doi: 10.1175/JAS-D-11-0276.1.].

Bister, M. and K. A. Emanuel, 1998: Dissipative heating and hurricane intensity. *Meteor. Atmos. Phys.*, **52**, 233–240.

Bister, M. and K. A. Emanuel, 2002: Low frequency variability of tropical cyclone potential intensity 1. Interannual to interdecadal variability. *J. Geophys. Res.*, **107**, 26.1–26.15.

Bryan, G. H. and M. Fritsch, 2002: A benchmark simulation for moist nonhydrostatic numerical models. *Mon. Wea. Rev.*, **130**, 2917–2928.

Bu, Y. P., R. G. Fovell, and C. K. L., 2014: Influence of cloud-radiative forcing on tropical cyclone structure. *J. Atmos. Sci.*, **71**, 1644–1662, doi: 10.1175/JAS-D-13-00265.1.

Camp, J. P. and M. T. Montgomery, 2001: Hurricane maximum intensity: past and present. *Mon. Wea. Rev.*, **129**, 1704–1717.

Craig, G., 1996: Numerical experiments on radiation and tropical cyclones. **122**, 415–422, doi: 10.1002/qj.49712253006.

DeMaria, M. and J. Kaplan, 1994: A Statistical Hurricane Intensity Prediction Scheme (SHIPS) for the Atlantic basin. *Wea. Forecasting*, **9**, 209–220.

DeMaria, M. and J. Kaplan, 1999: An updated Statistical Hurricane Intensity Prediction Scheme (SHIPS) for the Atlantic and eastern North Pacific basins. *Wea. Forecasting*, **14**, 326–337.

Doyle, J. D. and Coathors, 2017: A view of tropical cyclones from above. *Bull. Amer. Meteor. Soc.*, **74**, 2113–2134, doi: 10.1175/BAMS-D-16-0055.1.

Dudhia, J., 1989: Numerical study of convection observed during the winter monsoon experiment using a mesoscale two dimensional model. *J. Atmos. Sci.*, **46**, 3077–3107, doi: 10.1175/1520-0469(1989)046<3077:NSOCOD>2.0.CO;2.

Dunion, J. P., C. D. Thorncroft, and V. C. S., 2014: The tropical cyclone diurnal cycle of mature hurricanes. *Mon. Wea. Rev.*, **142**, 3900–3919, doi: 10.1175/MWR-D-13-00191.1.

Duran, P. and J. Molinari, 2018: Dramatic inner-core tropopause variability during the rapid intensificaiton of Hurricane Patricia (2015). *Mon. Wea. Rev.*, **146**, 119–134, doi: 10.1175/MWR-D-17-0218.1.

Eliassen, A., 1952: Slow thermally or frictionally controlled meridional circulations in a circular vortex. *Astrophys. Norv.*, **5**, 19–60.

Emanuel, K. and R. Rotunno, 2011: Self-stratification of tropical cyclone outflow. part I: implications for storm structure. *J. Atmos. Sci.*, **68**, 2236–2249, doi: 10.1175/JAS-D-10-05024.1.

Emanuel, K. A., 1986: An air-sea interaction theory for tropical cyclones. Part I: Steady state maintenance. *J. Atmos. Sci.*, **43**, 585–604.

Emanuel, K. A., 1988: The maximum intensity of hurricanes. *J. Atmos. Sci.*, **45**, 1143–1155.

Emanuel, K. A., 1989: The finite-amplitude nature of tropical cyclogenesis. *J. Atmos. Sci.*, **46**, 3431–3456.

Emanuel, K. A., 1997: Some aspects of hurricane inner-core dynamics and energetics. *J. Atmos. Sci.*, **54**, 1014–1026.

Emanuel, K. A., 2003: Tropical cyclones. *Annu. Rev. Earth Planet. Sci.*, **31**, 75–104, doi: 10.1146/annurev.earth.31.100901.141259.

Emanuel, K. A., 2004: Tropical cyclone energetics and structure. *Atmospheric Turbulence and Mesoscale Meteorology*, E. Fedorovich, R. Rotunno, and B. Stevens, Eds., Cambridge University Press, 280.

Emanuel, K. A., 2012: Self-stratification of tropical cyclone outflow. Part II: Implications for storm intensifications. *J. Atmos. Sci.*, **69**, 988–996, doi: 10.1175/JAS-D-11-0177.1.

Emanuel, K. A., S. Solomon, D. Folini, S. Davis, and C. Cagnazzo, 2013: Influence of tropical tropopause layer cooling on atlantic hurricane activity. *J. Climate*, **26**, 2288–2301, doi: 10.1175/jcli-d-12-00242.1.

Fovell, R. G., K. L. Bu, Y. P. Corbosiero, W. Tung, Y. Cao, H. Kuo, L. Hsu, and H. Su, 2016: Influence of cloud microphysics and radiation on tropical cyclone structure and motion. *Meteor. Monogr.*, **56**, 11.1–11.27, doi: 10.1175/AMSMONOGRAPHS-D-15-0006.1.

Fovell, R. G., K. L. Corbosiero, A. Seifert, and K.-N. Liou, 2010: Impact of cloud-radiative processes on hurricane track. *Geophys. Res. Lett.*, **37**, doi: 10.1029/2010GL042691.

Gettelman, A. and P. d. F. Forster, 2002: A climatology of the tropical tropopause layer. *J. Meteor. Soc. Japan*, **80**, 911–924.

Godbole, R. V., 1973: On destabilization of clouds by radiative cooling. *Mon. Wea. Rev.*, **101**, 496–500.

Gray, W. M. and R. W. Jacobson, Jr., 1977: Diurnal variation of deep cumulus convection. *Mon. Wea. Rev.*, **105**, 1171–1188, doi: 10.1175/1520-0493(1977)105,1171:DVODCC.2.0.CO;2.

Hakim, G. J., 2011: The mean state of axisymmetric hurricanes in statistical equilibrium. *J. Atmos. Sci.*, **68**, 1364–1376, doi: 10.1175/2010JAS3644.1.

Holland, G. J., 1997: The maximum potential intensity of tropical cyclones. *J. Atmos. Sci.*, **54**, 2519–2541, doi: 10.1175/1520-0469(1997)054<2519:TMPIOT>2.0.CO;2.

Hong, S.-Y., Y. Noh, and J. Dudhia, 2006: A new vertical diffusion package with an explicit treatment of entrainment processes. *Mon. Wea. Rev.*, **134**, 2318–2341, doi: 10.1175/MWR3199.1.

Kleinschmidt, E., 1951: Grundlagen einer theorie der tropeschen zyklonen. *Arch. Meteor. Geophys. Bioklimatol.*, **A4**, 53–72.

Melhauser, C. and F. Zhang, 2014: Diurnal radiation cycle impact on the pregenesis environment of hurricane karl (2010). *J. Atmos. Sci.*, **71**, 1241–1259, doi: 10.1175/JAS-D-13-0116.1.

Mlawer, E. J., S. J. Taubman, P. D. Brown, M. J. Iacono, and S. A. Clough, 1997: Radiative transfer for inhomogeneous atmospheres: RRTM, a validated correlated-k model for the longwave. *J. Geophys. Res.*, **102**, 16 663–16 682, doi: 10.1029/97JD00237.

Navarro, E. L. and G. J. Hakim, 2016: Idealized numerical modeling of the diurnal cycle of tropical cyclones. *J. Atmos. Sci.*, **73**, 4189–4201, doi: 10.1175/JAS-D-15-0349.1.

Navarro, E. L., G. J. Hakim, and H. E. Willoughby, 2017: Balanced response of an axisymmetric tropical cyclone to periodic diurnal heating. *J. Atmos. Sci.*, **74**, 3325–3337, doi: 10.1175/JAS-D-16-0279.1.

Nicholls, M. E., 2015: An investigation of how radiation may cause accelerated rates of tropical cyclogenesis and diurnal cycles of convective activity. *Atmos. Chem. Phys.*, **15**, 9003–9029, doi: 10.5194/acp-15-9003-2015.

Nie, J. and H. Sobel, 2015: Responses of tropical deep convection to the QBO: Cloud-resolving simulations. *J. Atmos. Sci.*, **72**, 3625–3638, doi: 10.1175/JAS-D-15-0035.1.

Nolan, D. S., 2007: What is the trigger for tropical cyclogenesis? *Aust. Meteor. Mag.*, **56**, 241–266.

Ohno, T., M. Satoh, and Y. Yamada, 2016: Warm core, eyewall slopes, and intensities of tropical cyclones simulated by a 7-km-mesh global nonhydrostatic model. *J. Atmos. Sci.*, **73**, 4289–4309, doi: 10.1175/JAS-D-15-0318.1.

Ramsay, H. A., 2013: The effects of imposed stratospheric cooling on the maximum intensity of tropical cyclones in axisymmetric radiative-convective equilibrium. **26**, 9977–9985, doi: 10.1175/JCLI-D-13-00195.1.

Rogers, D. P. and D. Karacin, 1992: Radiative transfer and turbulence in the cloud-topped marine atmospheric boundary layer. *J. Atmos. Sci.*, **49**, 1473–1486.

Rotunno, R. and K. A. Emanuel, 1987: An air-sea interaction theory for tropical cyclones. Part II: Evolutionary study using a nonhydrostatic axisymmetric numerical model. *J. Atmos. Sci.*, **44**, 542–561, doi: 10.1175/1520-0469(1986)043<0585:AASITF>2.0.CO;2.

Saha, S. and Coathors, 2010: The NCEP climate forecast system reanalysis. *Bull. Amer. Meteor. Soc.*, **91**, 1015–1057, doi: 10.1175/2010BAMS3001.1.

Schmetz, J. and M. Beniston, 1986: Relative effects of solar and infrared radiative forcing in a mesoscale model. *Boundary. Layer. Meteor.*, **34**, 137–155.

Seidel, D. J., R. Ross, J. K. Angell, and G. C. Reid, 2001: Climatological characteristics of the tropical tropopause as revealed by radiosondes. *J. Geophys. Res.*, **106**, 7857–7878, doi: 10.1029/2000JD900837.

Skamarock, W. C. and Coauthors, 2008: *A description of the Advanced Research WRF version 3*. NCAR Tech. Note NCAR/TN-475+STR, doi: 10.5065/D68S4MVH.

Sui, C.-H., A. Li, and K.-M. Lau, 1998: Radiative-convective processes in simulated diurnal variations of tropical oceanic convection. *J. Atmos. Sci.*, **55**, 2345–2357.

Sundqvist, H., 1970: Numerical simulation of the development of tropical cyclones with a ten-level model. Part II. *Tellus*, **5**, 504–510.

Tang, B. and K. A. Emanuel, 2010: Midlevel ventilation's constraint on tropical cyclone intensity. *J. Atmos. Sci.*, **67**, 1817–1830, doi: 10.1175/2010JAS3318.1.

Tang, X. and F. Zhang, 2016: Impacts of the diurnal radiation cycle on the formation, intensity, and structure of Hurricane Edouard (2014). *J. Atmos. Sci.*, **73**, 2871–2892, doi: 10.1175/JAS-D-15-0283.1.

Thompson, G. and T. Eidhammer, 2014: A study of aerosol impacts on clouds and precipitation development in a large winter cyclone. *J. Atmos. Sci.*, **71**, 3636–3658, doi: 10.1175/JAS-D-13-0305.1.

Tiedtke, M., 1989: A comprehensive mass flux scheme for cumulus parameterization in large-scale models. *Mon. Wea. Rev.*, **117**, 1779–800, doi: 10.1175/1520-0493(1989)117<1779:ACMFSF>2.0.CO;2.

Van Sang, N., R. K. Smith, and M. T. Montgomery, 2008: Tropical cyclone intensification and predictability in three dimensions. *Quart. J. Roy. Meteor. Soc.*, **134**, 563–582, doi: 10.1002/qj.235.

Wang, S., S. J. Camargo, A. H. Sobel, and L. M. Polvani, 2014: Impact of the tropopause temperature on the intensity of tropical cyclones: An idealized study using a mesoscale model. *J. Atmos. Sci.*, **71**, 4333–4348, doi: 10.1175/JAS-D-14-0029.1.

Willoughby, H. E., 2009: Diabatically induced secondary flows in tropical cyclones. part II: Periodic forcing. *Mon. Wea. Rev.*, **137**, 822–835.

Wu, C.-C., H.-H. Wu, S.-N. aand Wei, and S. F. Abarca, 2016: The role of convective heating in tropical cyclone eyewall ring evolution. *J. Atmos. Sci.*, **73**, 319–330, doi: 10.1175/JAS-D-15-0085.1.

Xu, K.-M. and D. A. Randall, 1995: Impact of interactive radiative transfer on the macroscopic behavior of cumulus ensembles. part II: Mechanisms for cloud-radiation interactions. *J. Atmos. Sci.*, **52**, 800–817, doi: 10.1175/1520-0469(1995)052,0800: IOIRTO.2.0.CO;2.